5. Bacterial Patterns and Chemotaxis

5.1 Background and Experimental Results

There is an obvious case for studying bacteria. For example, bacteria are responsible for a large number of diseases and they are responsible for most of the recycling that takes place. Their use in other areas is clearly going to increase as our understanding of their complex biology becomes clearer. Here we are interested in how a global pattern in bacterial populations can arise from local interactions. Under a variety of experimental conditions numerous strains of bacteria aggregate to form stable (or rather temporarily stable) macroscopic patterns of surprising complexity but with remarkable regularity. It is not easy to explain how these patterns are formed solely by experiment, but they can, however, be explained for the most part, with the use of mathematical models based on the known biology. It is not possible to discuss all the patterns which have been studied experimentally so we concentrate on the collection of diverse patterns observed by Berg and his colleagues (see Budrene and Berg 1991, 1995 and earlier references there) in the bacteria *Escherichia coli* (*E. coli*) and *Salmonella typhimurium* (*S. typhimurium*).

E. coli and *S. typhimurium* are common bacteria: for example, *E. coli* is abundant in the human intestine and *S. typhimurium* can occur in incompletely cooked poultry and meat. These bacteria are motile and they move by propelling themselves by means of long hairlike flagella (Berg 1983). Berg also mapped the movement of a bacterium over time, and found that the organism's motion approximates a random walk and so the usual Fickian diffusion can be used to describe their random motility; their diffusion coefficient has been measured experimentally.

A key property of many bacteria is that in the presence of certain chemicals they move preferentially towards higher concentration of the chemical, when it is a chemoattractant, or towards a lower concentration when it is a repellent. The sensitivity to such gradients often depends on the concentration levels. In the modelling below we shall be concerned with chemotaxis and the sensitivity issue. The basic concept of chemotaxis (and diffusion) was discussed in Chapter 11, Volume I, Section 11.4 and in more detail in the last chapter. Basically, whether or not a pattern will form depends on the appropriate interplay between the bacterial populations and the chemical kinetics and the competition between diffusive dispersal and chemotactic aggregation.

Budrene and Berg (1991, 1995) carried out a series of experimental studies on the patterns that can be formed by *S. typhimurium* and *E. coli*. They showed that a bacterial colony can form interesting and remarkably regular patterns when they feed on, or are

exposed to, intermediates of the tricarboxylic acid (TCA) cycle especially succinate and fumarate. They used two experimental methods which resulted in three pattern forming mechanisms. The bacteria are placed in a liquid medium in one procedure, and on a semi-solid substrate (0.24% water agar) in the other. They found one mechanism for pattern formation in the liquid medium, and two in the semi-solid medium. In all of the experiments, the bacteria are known to secrete aspartate, a potent chemoattractant.

Liquid Experiments with E. coli and S. typhimurium

These experiments produce relatively simple patterns which appear quickly, on the order of minutes, and last about half an hour before disappearing permanently. Two types of patterns are observed and are selected according to the initial conditions. The simplest patterns are produced when the liquid medium contains a uniform distribution of bacteria and a small amount of the TCA cycle intermediate. The bacteria collect in aggregates of roughly the same size over the entire surface of the liquid, although the pattern often starts in one general area and spreads from there (Figure 5.1(a)).

In the second type of liquid experiment, the initial density of bacteria is uniform, and the TCA cycle intermediate is added locally to a particular spot, referred to as the 'origin.' Subsequently, the bacteria are seen to form aggregates which occur on a ring centred about the origin, and in a random arrangement inside the ring (Figure 5.1(b)).

Importantly, in these liquid experiments, the patterns are generated on a timescale which is less than the time required for bacterial reproduction and so proliferation does not contribute to the pattern formation process. Also, the bacteria are not chemotactic to any of the chemicals initially placed in the medium, including the stimulant. The experimentalists (H.C. Berg, personal communication 1994) also confirmed that fluid dynamic effects are not responsible for the observed patterns.

Semi-Solid Experiments with E. coli and S. typhimurium

The most interesting patterns are observed in the semi-solid experiments and in particular with *E. coli*. For these experiments, a high density inoculum of bacteria is placed on a petri dish which contains a uniform distribution of stimulant in the semi-solid medium, namely, 0.24% water agar. Here the stimulant also acts as the main food source for the bacteria, and so the concentrations are much larger than in the liquid experiments. After two or three days, the population of bacteria has gone through 25–40 generations during which time it spreads out from the inoculum, eventually covering the entire surface of the dish with a stationary pattern of high density aggregates separated by regions of near zero cell density. Some typical final patterns are shown in Figures 5.2 and 5.3. The *S. typhimurium* patterns are concentric rings and are either continuous or spotted while *E. coli* patterns are more complex, involving a greater degree of positional symmetry between individual aggregates. An enormous variety of patterns has been observed, the most common being sunflower type spirals, radial stripes, radial spots and chevrons. Using time-lapse videography of the experiments reveals the very different kinematics by which *S. typhimurium* and *E. coli* form their patterns.

The simple *S. typhimurium* patterns (Figure 5.2) begin with a very low density bacterial lawn spreading out from the initial inoculum. Some time later, a high density ring of bacteria appears at some radius less than the radius of the lawn and after another

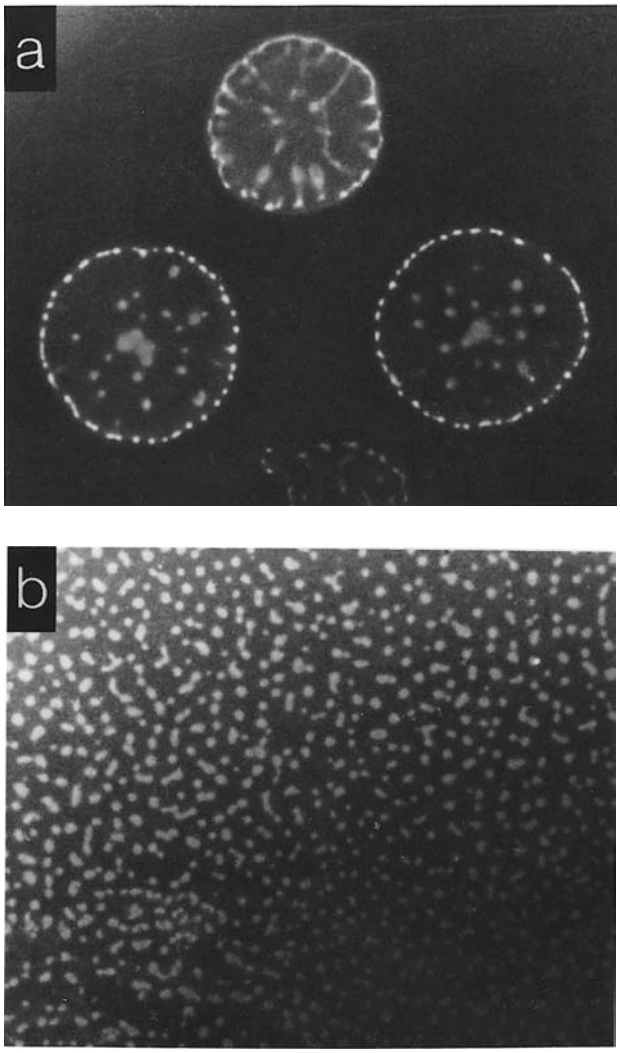

Figure 5.1. Bacterial patterns formed by *Salmonella typhimurium* in liquid medium. (**a**) A small amount of TCA was added to a uniform distribution of bacteria. (**b**) A small amount of TCA was added locally to a uniform distribution of bacteria. (Unpublished results of H. Berg and E.O. Budrene; photographs were kindly provided by courtesy of Dr. Howard Berg and Dr. Elena Budrene and reproduced with their permission.)

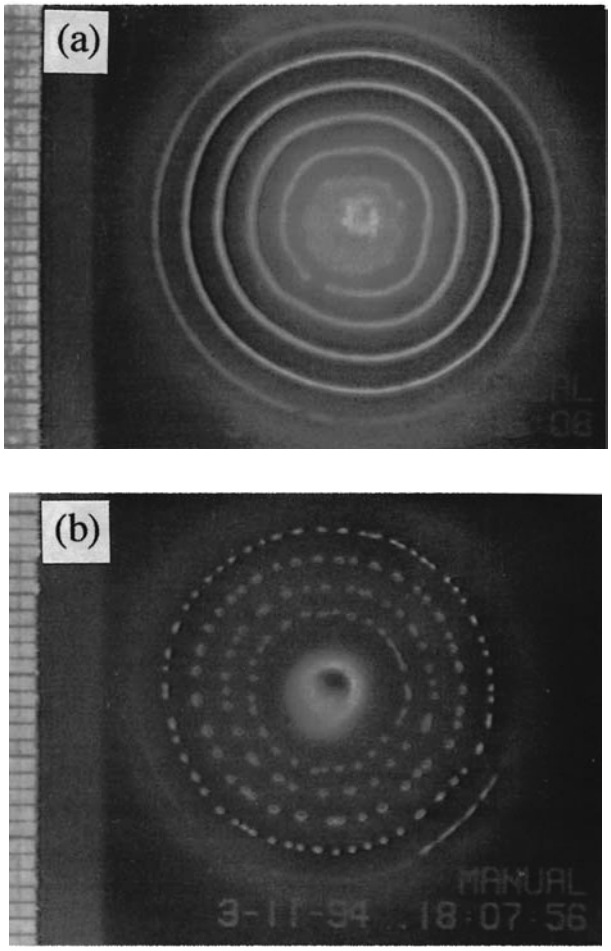

Figure 5.2. Typical *S. typhimurium* patterns obtained in semi-solid medium and visualized by scattered light. Experiments were carried out by Howard Berg and Elena Budrene using the techniques described in Budrene and Berg (1991). About 10^4 bacteria were inoculated at the centre of the dish containing 10 ml of soft agar in succinate. In (**a**) the rings remain more or less intact while in (**b**) they break up as described in the text: the time from inoculation in (**a**) is 48 hours and in **(b)**, 70 hours. The 1-mm grid on the left of each figure gives an indication of the scale of the patterns. (From Woodward et al. 1995 where more experimental details and results are provided)

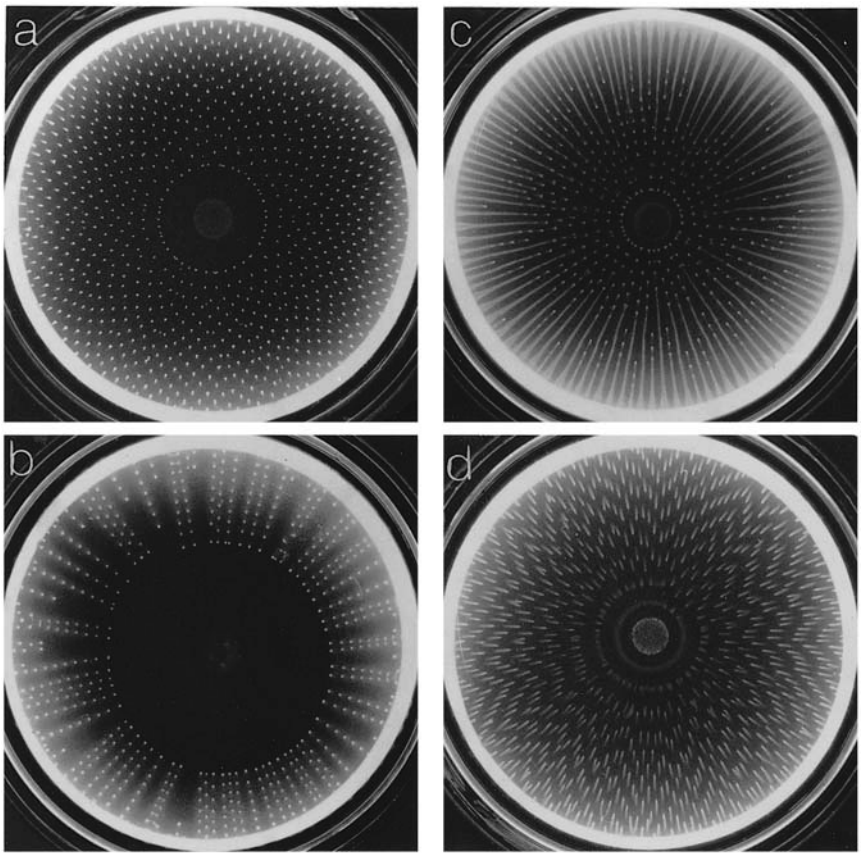

Figure 5.3. *E. coli* patterns obtained in semi-solid medium. Note the highly regular patterns. The light regions represent high density of bacteria. The different patterns (**a**)–(**d**) are discussed in the text at several places. (From Budrene and Berg (1991); photographs courtesy of Dr. Howard Berg and reproduced with permission)

time interval, when the lawn has expanded further, a second high density bacterial ring appears at some radius larger than that of the first ring. The rings, once they are formed, are stationary. The rings may remain continuous as in Figure 5.2(a) or break up into a ring of spots as in Figure 5.2(b). The high density aggregates of bacteria in one ring have no obvious positional relation to the aggregates in the two neighbouring rings.

The more dramatic patterns exhibited by *E. coli*, such as those shown in Figure 5.3, have definite positional relationships between radially and angularly neighbouring aggregates. These relationships seem to be the result of existing aggregates inducing the formation of subsequent ones (Budrene and Berg 1995). Instead of an initial bacterial lawn, a swarm ring of highly active motile bacteria forms and expands outwards from the initial inoculum. The bacterial density in the swarm ring increases until the ring becomes unstable and some percentage of the bacteria are left behind as aggregates. These aggregates remain bright and full of vigorously motile bacteria for a short time, but then dissolve as the bacteria rejoin the swarm ring. Left behind in the aggregate's original

location is a clump of bacteria which, for some unknown reason, are non-motile: it is these non-motile bacteria that are the markers of the pattern.

It appears that one, or both, of the speed of the swarm ring and the time at which the dissolution of aggregates occurs, are key elements in the formation of any one pattern. If the dissolution happens quickly, the aggregates appear to be pulled along by the swarm ring, and the non-motile bacteria are left behind as a radial streak as in Figures 5.3(c) and (d). On the other hand if the dissolution happens a little less quickly, the cells from the dissolved aggregate rejoin the swarm ring and induce the formation of aggregates at the rejoining locations and this results in a radial spot pattern. If the dissolution happens even more slowly, the swarm ring becomes unstable before the bacteria from the aggregates have time to rejoin the ring. The ring then tends to form aggregates in between the locations where aggregates already exist which results in a sunflower spiral type of pattern.

Remember that, just as in the liquid experiments, none of the chemicals placed in the petri dish is a chemoattractant. The timescale of these patterns, however, is long enough to accommodate several generations of *E. coli*, and so proliferation is important here. Consumption of stimulant is also non-negligible, especially in the swarm ring patterns.

Since none of the substrates used are chemoattractants the patterns of *E. coli* in Figure 5.3 cannot be explained by some external chemoattractants. Chemoattractants, however, play a major role since the bacteria themselves produce a potent chemoattractant, namely, aspartate (Budrene and Berg 1991). Up to this time it had been assumed that the phenomenon of chemotaxis existed in *E. coli* and *S. typhimurium* only to guide the bacteria towards a food source. It was only in these experiments of Budrene and Berg (1991, 1995) that evidence was found that the bacteria can produce and secrete a chemoattractant as a signalling mechanism. This is reminiscent of the slime mould *Dictyostelium discoideum* where the cells produce the chemical cyclic AMP as a chemotactic aggregative signalling mechanism. In our modelling therefore we focus primarily on the processes of diffusion and chemotaxis towards an endogenously produced chemoattractant and how they interact to produce the bacterial patterns.

We should remember that all of these patterns are formed on a two-dimensional domain of the petri dish. With the wide variety of patterns possible it is clear that if the medium were three-dimensional the pattern complexity would be even greater. It would be quite an experimental challenge to photograph them. Here we model only the two-dimensional patterns and show that the models, which reflect the biology, can create the experimentally observed patterns.

What is clear is that chemotaxis phenomena can give rise to complex and varied geometric patterns. How these complex geometries form from interactions between individual bacteria is not easy to determine intuitively from experiments alone.[1] In cases such as this, when biological intuition seems unable to provide an adequate explanation, mathematical modelling can play an important, even crucial, role. To understand the patterns, many questions must be answered, often associated with the fine details of the biological assumptions and parameter estimates. For example, are diffusion and

[1] It was for this reason that Howard Berg initially got in touch with me. A consequence of the first joint modelling attempts (Woodward et al. 1995) generated informative and interesting experimental and biological questions.

chemotaxis towards an endogenously produced chemoattractant sufficient to explain the formation of these patterns? What is the quantitative role of the chemoattractant stimulant and how quickly must it be produced? What other patterns are possible and what key elements in the experiments should be changed to get them? A review of the biology, the modelling and the numerical schemes used to simulate the model equations is given by Tyson (1996).

Most of the material we consider in detail is based on a series of theoretical studies of these specific patterns (Woodward et al. 1995, Tyson 1996, Murray et al. 1998, Tyson et al. 1999). They proposed mathematical models which closely mimic the known biology. Woodward et al. (1995)—a collaborative work with the experimentalists Drs. Berg and Budrene—considered the less complex patterns formed by *S. typhimurium* and proposed an explanation for the observed self-organization of the bacteria. Ben-Jacob and his colleagues (Ben-Jacob et al. 1995, 2000; see other references there) have also studied a variety of bacteria both theoretically and experimentally: many of the patterns they obtain are also highly complex and dramatic. The patterns depend, of course, on the parameter values and experimental conditions. In nature, however, bacteria have to deal with a variety of conditions, both hostile and friendly. To accommodate such environmental factors bacteria have developed strategies for dealing with such conditions. These strategies involve cooperative communication and this affects the type of patterns they form. Ben-Jacob (1997; see other references there) has investigated the effect of possible communication processes, such as chemotactic feedback. The consequences of including such cooperativity in the model chemotactic systems is, as would be expected, that the spectrum of pattern complexity is even greater. The analytical and extensive numerical studies of Mimura and his colleagues (see, for example, Mimura and Tsujikawa 1996, Matsushita et al. 1998, 1999, Mimura et al. 2000 and other references there) are particularly important in highlighting some of the complex solution behaviour reaction diffusion chemotaxis systems can exhibit. For example, Mimura et al. (2000) classify the various pattern classes (five of them) and suggest that, with one exception, the morphological diversity can be generated by reaction diffusion models. Mimura and Tsujikawa (1996) considered a diffusion-chemotaxis with population growth and in the situation of small diffusion and chemotaxis they derived an equation for the time evolution of the aggregating pattern. In this chapter we discuss specific bacterial patterns obtained with *S. typhimurium* and *E. coli* and, very briefly, those exhibited by *Bacillus subtilis* which are quite different.

These bacterial patterns are far more elaborate than those observed when chemotactic strains grow on media containing nutrients that are attractants (for example, Agladze et al. 1993). They also differ from the travelling waves of aggregating cells of the slime mould *Dictyostelium discoideum* in that the structures formed by *E. coli* and *S. typhimurium*, for example, are only temporally stable.

The spatial pattern potential of chemotaxis has been exploited in a variety of different biological contexts. Mathematical models involving chemotaxis (along with reaction diffusion models (Chapters 2 and 3) and mechanochemical models (Chapters 6 and 7) are simply part of the general area of integrodifferential equation models for the development of spatial patterns. The basic Keller–Segel continuum mechanism for pattern formation in the slime mould *Dictyostelium discoideum* was proposed by Keller and Segel (1970) and was discussed in Chapter 11, Volume I, Section 11.4. A discrete, more

biologically based, model (as a consequence of the new biological insights found since then) for the aggregation with appropriate cell signalling is given by Dallon and Othmer (1997). Othmer and Schaap (1998) give an extensive and thorough review of oscillatory cyclic AMP signalling in the development of this slime mould. Since the pioneering work of Keller and Segel (1970, 1971), a considerable amount of modelling effort has been expended on these patterns such as the work on bacteria by Ben-Jacob et al. (1995) who had thresholding behaviour in aspartate production and a cell-secreted waste field in their model. They obtained spatial patterns resembling some of the experimentally observed *E. coli* patterns. Brenner et al. (1998) performed a one-dimensional analysis of a model mechanism for swarm ring formation of *E. coli* patterns in a semi-solid medium. They studied the relative importance of the terms in their equations from the point of view of pattern formation and obtained some analytical results: for example, they derived an expression for the number of clumps in a given domain in terms of the model parameters.

Chemotaxis plays an important role in a wide range of practical phenomena such as in wound healing (see Chapter 10), cancer growth (see Chapter 11) and leukocytes moving in response to bacterial inflammation (for example, Lauffenburger and Kennedy 1983 and Alt and Lauffenburger 1987). Until recently, relatively little work had been done where cell populations are not constant; one exception was the travelling wave model of Kennedy and Aris (1980) where the bacteria reproduce and die as well as migrate. It appears that the presence of chemotaxis (or haptotaxis, a similar guidance phenomenon for cells in the mechanical theory of pattern formation discussed in Chapter 6) results in a wider variety of patterns than only reaction and diffusion, for example. Of course, when significant growth occurs during the patterning process the spectrum of patterns is even wider.

It is possibly pertinent to note here that the specific patterns formed by many bacteria depend sensitively on the parameters and on the conditions that obtain in the experiments, including the initial conditions. As such a potential practical application of bacterial patterning is as a quantitative measurement of pollution.

5.2 Model Mechanism for *E. coli* in the Semi-Solid Experiments

Basically we want to construct the biological mechanisms which govern the bacterial pattern formation processes in the experiments of Budrene and Berg (1991, 1995). We first consider the model for the semi-solid medium experiment with *E. coli*. The key players in the experiment seem to be the bacteria (of course), the chemoattractant (aspartate) and the stimulant (succinate or fumarate) so we consider the three variables: the cell density, n, the chemoattractant concentration, c, and the stimulant concentration, s. The bacteria diffuse, move chemotactically up gradients of the chemoattractant, proliferate and become non-motile. The non-motile cells can be thought of as dead, for the purpose of the model. The chemoattractant diffuses, and is produced and ingested by the bacteria while the stimulant diffuses and is consumed by the bacteria. To begin with it is usually helpful to simply write down a word equation for what you think is going

on.[2] From the description of the biological processes described in the last section we suggest the following model consisting of three conservation equations of the form

$$\boxed{\text{rate of change of cell density, } n} = \boxed{\text{diffusion of } n} + \boxed{\text{chemotaxis of } n \text{ to } c} + \boxed{\text{proliferation (growth and death) of } n} \tag{5.1}$$

$$\boxed{\text{rate of change of chemoattractant concentration, } c} = \boxed{\text{diffusion of } c} + \boxed{\text{production of } c \text{ by } n} - \boxed{\text{uptake of } c \text{ by } n} \tag{5.2}$$

$$\boxed{\text{rate of change of stimulant concentration, } s} = \boxed{\text{diffusion of } s} - \boxed{\text{uptake of } s \text{ by } n} \tag{5.3}$$

The crucial part of the modelling is how to quantify the individual terms in these equations. A full discussion of the modelling is given by Tyson (1996) who also estimates the various parameters which appear from an extensive literature survey. It is mainly her work together with that in Tyson et al. (1999) and Murray et al. (1998) that we discuss here.

Diffusion

The diffusion terms for the chemoattractant and the stimulant in (5.2) and (5.3) are straightforward. These chemicals diffuse according to simple Fickian diffusion with diffusion coefficients D_c and D_s respectively with estimates (H.C. Berg, personal communication 1993)

$$D_c \approx D_s \approx 9 \times 10^{-6} \text{ cm}^2 \text{ s}^{-1}.$$

All the parameter estimates are gathered together in Table 5.1 below.

We assume that the bacteria as a population also diffuse in a Fickian manner. The estimation of their diffusion coefficient, D_n, however, is less straightforward. In his book, Berg (1983) gives an expression for the diffusion constant of bacteria derived from the individual motion of the cells and comes up with an estimate of $D_n \approx 2 \times 10^{-6}\text{cm}^2\text{s}^{-1}$. Phillips et al. (1994) catalogued values of the diffusion coefficient reported in the literature over the previous 10 years: the values range from $D_n \approx 1.9\,(\pm 0.9) \times 10^{-4}$ cm^2 s^{-1} at the upper end to $D_n \approx$ 1–10 $\times\ 10^{-7}$ cm^2 s^{-1} at the lower end. The most recent measurements, however, fall in the range $D_n \approx$ 1–3 $\times\ 10^{-6}$ cm^2 s^{-1}, which corresponds with the theoretical value determined by Berg (1983).

In deciding on the appropriate diffusion coefficient for the model, we must keep in mind the number of space dimensions for movement which were available to the bacteria when the measurements were made. In the experiments we model, the depth of the liquid or agar mixture in the petri dish is of the order of 1.8 mm. When restricted

[2] It is essential when discussing with experimentalists who have little experience of mathematical modelling.

to motion through 10-mm capillary arrays, *E. coli* diffuse with a diffusion coefficient of 5.2×10^{-6} cm^2 s^{-1}, while through 50-mm capillary arrays, the diffusion coefficient was found to be 2.6×10^{-6} cm^2 s^{-1} (Berg and Turner, 1990). As we would expect, diffusion through the larger capillaries is slower.

Estimating diffusion coefficients of cells or bacteria, or really anything other than chemicals, is always a problem (see also Chapters 9, 10, 11, 13, and 14). A variety of theoretical approaches has been used to estimate diffusion coefficients such as that by Sherratt et al. (1993b) in their study of eukaryotic cell movement. Ford and Lauffenburger (1991) and Sherratt (1994) developed models beginning with receptor level kinetics in their analysis to determine the diffusion coefficient of bacteria.

For our purposes, it is not necessary to include such receptor level detail since the experimentalists believe that the absolute chemoattractant concentration does not affect the diffusion coefficient of the bacteria. So, we assume the cells diffuse with a constant diffusion coefficient with a value $D_n = 2\text{–}4 \times 10^{-6}$cm^2 s^{-1}.

Chemotaxis

Chemotaxis, as we saw in Chapter 11, Volume I, involves the directed movement of organisms up a concentration gradient, and so is like a negative diffusion. However, whereas diffusion of cells depends only on their density gradient, chemotaxis depends on the interaction between the cells, the chemoattractant and the chemoattractant gradient. The general form of the chemotaxis term in the conservation equations is the divergence of the chemotactic flux:

$$\nabla \cdot \mathbf{J_c} = \nabla \cdot [\chi(n, c)\nabla c], \tag{5.4}$$

where $\mathbf{J_c}$ is the chemotactic flux, $\chi(n, c)$ is the chemotaxis response function, as yet unknown, with n and c the cell density and chemoattractant concentration respectively. A lot of research has been directed to finding a biologically accurate expression for the chemotaxis function $\chi(n, c)$. Ford and Lauffenburger (1991) reviewed the main types of functions tried. As in the case of the diffusion term, forms for $\chi(n, c)$ have been proposed either by working up from a microscopic description of cell behaviour, or by curve fitting to macroscopic results from population experiments. A synthesis of the various approaches suggests that the macroscopic form of Lapidus and Schiller (1976), namely,

$$\chi(n, c) = \frac{n}{(k + c)^2},$$

where k is a parameter is a good one. This seems to give the best results when compared to experimental data, in particular the experiments by Dahlquist et al. (1972) which were designed specifically to pinpoint the functional form of the chemotactic response. Interestingly, the inclusion of all of the receptor level complexity by other researchers did not give any significant improvement over the results of Lapidus and Schiller (1976). The main advantage, a significant one of course, of receptor models is that the parameters can be directly applied to experimentally observable physicochemical properties of the bacteria. It is not necessary, however, to include such detail in a population study. For

the modelling and analyses here we are primarily interested in describing the behaviour of the populations of *E. coli* and *S. typhimurium* as a whole, so a macroscopically derived chemotaxis coefficient is most appropriate. Based on the above form, we choose (Woodward et al. 1995)

$$\chi(n, c) = \frac{k_1 n}{(k_2 + c)^2}. \tag{5.5}$$

The parameters k_1 and k_2 can be determined from the experimental results of Dahlquist et al. (1972) and give $k_2 = 5 \times 10^{-6}$ M and $k_1 = 3.9 \times 10^{-9}$ M cm^{2}s^{-1}.

Cell Proliferation

The proliferation term involves both growth and death of the bacteria. From Budrene and Berg (1995) cells grow at a constant rate that is affected by the availability of succinate. In the semi-solid experiments the stimulant, succinate or fumarate, is the main carbon source (nutrient) for the bacteria whereas in the liquid experiments, nutrient is provided in other forms and is not limiting. We thus assume a proliferation term of the form

$$\text{cell growth and death} = k_3 n \left(k_4 \frac{s^2}{k_9 + s^2} - n \right), \tag{5.6}$$

where the k's are parameters.

Intuitively this form is a reasonable one to take: it looks like logistic growth with a carrying capacity which depends on the availability of nutrient, s. When the bacterial density is below the carrying capacity, the expression (5.6) is positive and the population of bacteria increases. When n is larger than the carrying capacity, the expression is negative and there is a net decrease in population density. Implied in this form is the assumption that the death rate per cell is proportional to n; another possibility, but less plausible perhaps, is simply a constant death rate per cell.

Production and Consumption of Chemoattractant and Stimulant

The model contains one production term (production of chemoattractant), and two consumption terms (uptake of chemoattractant and of stimulant). Due to lack of available data, we have to rely on intuition to decide what are reasonable forms for the production and uptake of chemoattractant.

For the nutrient consumption, we expect that nutrient will disappear from the medium at a rate proportional to that at which cells are appearing. Since the linear birth rate of the cells is taken to be $k_3 k_4 s^2/(k_9 + s^2)$ this suggests the following form for the consumption of nutrient by the cells,

$$\text{nutrient consumption} = k_8 n \frac{s^2}{k_9 + s^2}, \tag{5.7}$$

where the k's are parameters. The consumption form has a sigmoid-like characteristic.

Chemoattractant consumption by the cells could have a similar sigmoidal character. However, the chemical is not necessary for growth and so there is likely very little created during the experiment. So, we simply assume that if a cell comes in contact with an aspartate molecule, it ingests it, which thus suggests a chemoattractant consumption, with parameter k_7, of the form

$$\text{chemoattractant consumption} = k_7 nc. \tag{5.8}$$

The chemoattractant production term has also not been measured in any great detail. We simply know (H.C. Berg, personal communication 1993) that the amount of chemoattractant produced increases with nutrient concentration and probably saturates over time which suggests a saturating function, of which there are many possible forms. To be specific we choose

$$\text{chemoattractant production} = k_5 s \frac{n^2}{k_6 + n^2}, \tag{5.9}$$

where k_5 and k_6 are other parameters. An alternative nonsaturating possibility which is also plausible is

$$\text{chemoattractant production} = k_5 s n^2. \tag{5.10}$$

In fact both these forms give rise to the required patterns, so further experimentation is needed to distinguish between them, or to come up with some other function. The critical characteristic is the behaviour when n is small since there the derivative of the production function must be positive.

Mathematical Model for Bacterial Pattern Formation in a Semi-Solid Medium

Let us now put these various functional forms into the model word equation system (5.1)–(5.3) which becomes:

$$\frac{\partial n}{\partial t} = D_n \nabla^2 n - \nabla \left[\frac{k_1 n}{(k_2 + c)^2} \nabla c \right] + k_3 n \left(\frac{k_4 s^2}{k_9 + s^2} - n \right) \tag{5.11}$$

$$\frac{\partial c}{\partial t} = D_c \nabla^2 c + k_5 s \frac{n^2}{k_6 + n^2} - k_7 nc \tag{5.12}$$

$$\frac{\partial s}{\partial t} = D_s \nabla^2 s - k_8 n \frac{s^2}{k_9 + s^2}, \tag{5.13}$$

where n, c and s are the cell density, the concentration of the chemoattractant and of the stimulant respectively. There are three diffusion coefficients, three initial values (n, c and s at $t = 0$) and nine parameters k in the model. We have estimates for some of these parameters while others can be estimated with reasonable confidence. There are several, however, which, with our present knowledge of the biology, we simply do not know. We discuss parameter estimates below.

Mathematical Model for Bacterial Pattern Formation in a Liquid Medium

It seems reasonable to assume that the production of chemoattractant and the chemotactic response of the cells are governed by the same functions in both the liquid and semi-solid experiments. The difference between the two groups of experiments lies more in the timescale and in the role of the stimulant. As mentioned earlier the cells do not have time to proliferate over the time course of the liquid experiments, so there is no growth term in this model. Also, the stimulant is not the main food source for the cells (it is externally supplied) so consumption of the stimulant is negligible. This shows that the liquid experiment model is simply a special case of the semi-solid experiment model. With cell growth, chemoattractant degradation and consumption of stimulant eliminated we are left with the simpler three-equation model

$$\frac{\partial n}{\partial t} = D_n \nabla^2 n - \nabla \left[\frac{k_1 n}{(k_2 + c)^2} \nabla c \right] \tag{5.14}$$

$$\frac{\partial c}{\partial t} = D_c \nabla^2 c + k_5 s \frac{n^2}{k_6 + n^2} \tag{5.15}$$

$$\frac{\partial s}{\partial t} = D_s \nabla^2 s \tag{5.16}$$

which has fewer unknown parameters than the semi-solid mode system. The last equation is uncoupled from the other equations. In the case of the simplest liquid experiment, in which the stimulant is uniformly distributed throughout the medium, the third equation can also be dropped.

Parameter Estimation

As mentioned, we have some of the parameter values and can derive estimates for others from the available literature; we also have estimates for some parameter combinations. The product $k_3 k_4$ is the maximum instantaneous growth rate, which is commonly determined from the generation time, t_{gen}, as

$$\text{instantaneous growth rate} = \frac{\ln 2}{t_{gen}}.$$

For the *E. coli* experiments, the generation time is of the order of 2 hours, giving an instantaneous growth rate of 0.35/hour. The grouping $k_3 k_4 / k_8$ is termed the yield coefficient, and is calculated by experimentalists as

$$Y = \frac{\text{weight of bacteria formed}}{\text{weight of substrate consumed}}.$$

Similarly, the grouping $k_3 k_4 / k_7$ is the yield coefficient for the bacteria as a function of chemoattractant (nitrogen source). The parameters k_1 and k_2 are calculated from measurements of cellular drift velocity and chemotaxis gradients made by Dahlquist et al. (1972).

Table 5.1. Dimensional parameter estimates obtained from the literature for use in the *E. coli* and *S. typhimurium* model equations (5.11)–(5.16). The other ks are unknown at this stage.

Parameter	Value	Source
k_1	3.9×10^{-9} M cm^{2}s^{-1}	Dahlquist et al. 1972
k_2	5×10^{-6} M	Dahlquist et al. 1972
k_3	1.62×10^{-9} hr ml^{-1}cell^{-1}	Budrene and Berg 1995
k_4	3.5×10^{8} cells ml^{-1}	Budrene and Berg 1995
k_9	4×10^{-6} M^2	Budrene and Berg 1995
D_n	$2 - 4 \times 10^{-6}$cm^{2}s^{-1}	Berg and Turner 1990; Berg 1983
D_c	8.9×10^{-6}cm^{2}s^{-1}	Berg 1983
D_s	$\approx 9 \times 10^{-6}$cm^{2}s^{-1}	Berg 1983
n_0	10^{8} cells ml^{-1}	Budrene and Berg 1991
s_0	$1 - 3 \times 10^{-3}$ M	Budrene and Berg 1995

Budrene and Berg (1995) measured growth rates for their experiments and this let us get reasonably precise determination of the parameters k_4, k_9 and k_3 by curve fitting. They also measured the ring radius as a function of time in the semi-solid experiments. The known parameter estimates are listed in Table 5.1 along with the sources used. We do not have estimates for the other parameters. However, since we shall analyse the equation sytems in their nondimensional form it will suffice to have estimates for certain groupings of the parameters. These are given below in the legends of the figures of the numerical solutions of the equations.

Intuitive Explanation of the Pattern Formation Mechanism

Before analysing any model of a biological problem it is always instructive to try and see intuitively what is going to happen in specific circumstances. Remember that the domain we are interested in is finite, the domain of the experimental petri dish. Consider the full model (5.11)–(5.13). In (5.13) the uptake term is a sink in a diffusion equation and so as time tends to infinity, the nutrient concentration, s, tends to zero. This in turn implies, from (5.11) and (5.12) that eventually cell growth and production of chemoattractant both tend to zero, while consumption of chemoattractant and death of cells continue. So, both the cell density and chemoattractant concentration also tend to zero as time tends to infinity. Thus the only steady state in this model is the one at which $(n, c, s) = (0, 0, 0)$ everywhere. But, of course, this is not the situation we are interested in. What it implies, though, is that it is not possible to carry out a typical linear analysis with perturbations about a uniform nonzero steady state. Instead we must look at the dynamic solutions of the equations.

Now consider the model system for the liquid experiments, equations (5.14)–(5.16). The last equation implies that eventually the stimulant will be spatially uniform since it is simply the classical diffusion equation which smooths out all spatial heterogeneities over time. By inspection there is a uniform steady state $(n, c, s) = (n_0, 0, 0)$ with n_0, the initial concentration of cells, being another parameter which can be varied experimentally. From (5.15) the source term is always positive so c will grow unboundedly.

In this case, eventually this concentration will be sufficiently high to significantly reduce the chemotaxis response in (5.14) and in the end simple diffusion is dominant and the solutions become time-independent and spatially homogeneous. So, again, with the liquid experiments, we have to look at the dynamic evolution of the solutions. Here a perturbation of any one of the steady states ($(n, c, s) = (n_0, 0, 0)$) results in a continually increasing concentration of chemoattractant. To get anything interesting from the model analyses therefore we have to look for patterns somewhere in that window of time between perturbation of the uniform initial conditions and saturation of the chemotactic response.

It is straightforward to see how the physical diffusion-chemotaxis system for the liquid model (5.14) to (5.16) could give rise to the appearance, and disappearance, of high density aggregates of cells. At $t = 0$ the cells begin secreting chemoattractant and since the cells are randomly distributed, some areas have a higher concentration of chemoattractant than others. Because of the chemotaxis these groups of higher cell concentration attract neighbouring cells, thereby increasing the local cell density, and decreasing it in the surrounding area. The new cells in the clump also produce chemoattractant, increasing the local concentration at a higher rate than it is being increased by the surrounding lower density cell population. In this way, peaks and troughs in cell density and chemoattractant concentration are accentuated. This is not the whole story since diffusion of the cells and the chemicals is also involved and this has a dispersive effect which tries to counter the aggregative chemotactic process and smooth out these peaks and troughs or rather prevent them happening in the first place. It is then the classical situation of local activation and lateral inhibition and which process dominates—aggregation or dispersion—depends on the intimate relation between the various parameters and initial conditions via n_0.

5.3 Liquid Phase Model: Intuitive Analysis of Pattern Formation

We saw in the last section in the discussion of the liquid experiments and their model system that patterns consisting of a random arrangement of spots will probably appear on a short timescale in the liquid medium experiments but eventually the aggregates fade and homogeneity again obtains. We suggested that this fading is probably due to saturation of the chemotactic response. Basically since cellular production of chemoattractant is not countered by any form of chemoattractant degradation (or inhibition), the amount of chemoattractant in the dish increases continuously. As a result, the chemotactic response eventually saturates, and diffusion takes over.

We also noted that the usual linear analysis about a uniform steady state is not possible so we have to develop a different analysis to study the pattern formation dynamics. The method (Tyson et al., 1999) we develop is very much intuitive rather than exact, but as we shall see it is nevertheless informative and qualitatively predictive and explains how transient patterns of randomly or circularly arranged spots can appear in a chemotaxis model and in experiment. We also give some numerical solutions to compare with the analytical predictions. For all of the analysis and simulations we assume zero flux boundary conditions which reflect the experimental situation.

We start with the simplest model for the liquid experiments which is just the semi-solid phase model with zero proliferation of cells, zero degradation of chemoattractant and uniform distribution of stimulant, s, which is neither consumed nor degraded and is thus just another parameter here. In these circumstances (5.14)–(5.16) become

$$\frac{\partial n}{\partial t} = D_n \nabla^2 n - k_1 \nabla \cdot \left[\frac{n}{(k_2 + c)^2} \nabla c \right] \tag{5.17}$$

$$\frac{\partial c}{\partial t} = D_c \nabla^2 c + k_5 s \frac{n^2}{k_6 + n^2}, \tag{5.18}$$

where n and c are respectively the density of cells and concentration of chemoattractant.

For simplicity the analysis we carry out is for the one-dimensional case where $\nabla^2 = \partial^2/\partial x^2$. Although we carry out the analysis for a one-dimensional domain the results can be extended with only minor changes to two dimensions (like what we did in Chapter 2 when investigating reaction diffusion pattern formation). We nondimensionalise the equations by setting

$$\begin{aligned} &u = \frac{n}{n_0}, \quad v = \frac{c}{k_2}, \quad w = \frac{s}{s_0}, \quad t^* = \frac{k_5 s_0}{k_2} t, \quad x^* = \left(\frac{k_5 s_0}{D_c k_2} \right)^{1/2} x, \\ &d = \frac{D_n}{D_c}, \quad \alpha = \frac{k_1}{D_c k_2}, \quad \mu = \frac{k_6}{n_0^2} \end{aligned} \tag{5.19}$$

which gives, on dropping the asterisks for algebraic simplicity, the nondimensional equations

$$\frac{\partial u}{\partial t} = d \frac{\partial^2 u}{\partial x^2} - \alpha \frac{\partial}{\partial x} \left[\frac{u}{(1 + v)^2} \frac{\partial v}{\partial x} \right] \tag{5.20}$$

$$\frac{\partial v}{\partial t} = \frac{\partial^2 v}{\partial x^2} + w \frac{u^2}{\mu + u^2}. \tag{5.21}$$

The quantities n_0 and s_0 (essentially parameters that can be varied experimentally) are the average initial cell density and concentration of stimulant respectively. Since the stimulant s is neither consumed nor degraded $w = 1$. Also, in the liquid experiments, since there is neither growth nor death in the cell population we have the conservation equation

$$\int_0^l u(x, t)\, dx = u_0 l,$$

where u_0 is the average initial nondimensional cell density which is 1 if n_0 is the initial uniform density. The dimensionless parameter values, listed in Table 5.2, are calculated using the dimensional parameter values listed in Table 5.1. The parameter μ is unknown. The initial conditions of the experiment are uniform nonzero cell density and

Table 5.2. Known and estimated values for the variables and dimensionless parameters used in the study of the *E. coli* and *S. typhimurium* liquid medium model (5.20) and (5.21).

Variable	Initial Value
u_0	1.0
w_0	1.0
v_0	0.0

Parameter	Value
α	80–90
d	0.25–0.5
μ	unknown

zero concentration of chemoattractant. We want to find solutions of (5.20) and (5.21) which are heterogeneous in space and which initially grow and then decay with time.

The nontrivial (that is, $u_0 \neq 0$) spatially independent solution of (5.20) and (5.21) with initial conditions $u(x,0) = 1$, $v(x,0) = 0$ is

$$u(x,t) = 1 \tag{5.22}$$

If we suppose that the initial conditions for (5.20) and (5.21) are small, $O(\varepsilon)$, random perturbations about the initial cell density, we look for solutions in the form

$$u(x,t) = 1 + \varepsilon f(t) \sum_k e^{ikx}, \quad v(x,t) = \frac{1}{\mu+1} t + \varepsilon g(t) \sum_k e^{ikx}, \tag{5.23}$$

where $0 < \varepsilon \ll 1$ and the k are the wavenumbers associated with the Fourier series of the random initial conditions. To approximate the actual experimental situation, where the initial concentration of chemoattractant is exactly zero, we set $g(0) = 0$. For illustration we choose $f(0) = 1$. We look for spatially varying solutions superimposed on the temporally growing solution.

Since we are looking for solutions on a finite domain with zero flux boundary conditions we have only sinusoidal (cosine) solutions involving only integer modes, m (cf. Chapter 2, Section 2.4), which are related to the wavenumbers, k, by

$$k^2 = \frac{m^2\pi^2}{l^2}, \tag{5.24}$$

where l is the dimensionless length of the domain. Substituting (5.23) into (5.20) and (5.21) and linearising (in ε) in the usual way we get, for each k, the $O(\varepsilon)$ equations

$$\frac{dF(\tau)}{d\tau} = -dk^2 F(\tau) + \alpha(\mu+1)^2 \frac{k^2}{\tau^2} G(\tau) \tag{5.25}$$

$$\frac{dG(\tau)}{d\tau} = -k^2 G(\tau) + \frac{2\mu}{(\mu+1)^2} F(\tau), \tag{5.26}$$

where $\tau = \mu + 1 + t$ (note that $\tau_0 = \tau_{t=0} = \mu + 1 > 0$), $F(\tau) \equiv f(t)$ and $G(\tau) \equiv g(t)$. The coefficient of the second term on the right-hand side of (5.25) is the only one which depends on the chemotaxis parameter α.

The analytical problem now is how to determine the solution behaviour of $F(\tau)$ and $G(\tau)$. It is clear from (5.25) that as $\tau \to \infty$ the coefficient of $G(\tau)$ tends to zero and the solution for $F(\tau)$ reduces to a decaying exponential. Once this happens, the solution of (5.26) also gives a decaying exponential. So, with the solution forms (5.23) the mechanism accounts for ultimate pattern disappearance with time. Let us now consider the growth of spatial pattern from the initial disturbance.

For τ near τ_0 (that is, t small) we can get more insight by combining (5.25) and (5.26) into a single second-order differential equation for the amplitude, $F(\tau)$, of the cell density pattern, to get

$$\frac{d^2F}{d\tau^2} + \left[k^2(d+1) + \frac{2}{\tau}\right]\frac{dF}{d\tau} + k^2\left(dk^2 + \frac{2d}{\tau} - \frac{2\alpha\mu}{\tau^2}\right)F = 0. \tag{5.27}$$

This has an exact solution in terms of confluent hypergeometric functions but it is essentially of zero practical use from the point of view of seeing what the solution behaviour is, which, after all, is what we want. Instead we use heuristic and qualitative reasoning. Without it, it would also be difficult to see what was actually going on if we simply solved the system numerically in the first instance. To begin we assume that the coefficients of the second-order ordinary differential equation (5.27) change much less rapidly than the function itself and its derivatives. This lets us compare (5.27) to a second-order equation with constant coefficients over small intervals of τ. Denote the coefficients of (5.27) by $D(\tau)$ and $N(\tau)$ and it becomes

$$\frac{d^2F}{d\tau^2} + D(\tau)\frac{dF}{d\tau} + N(\tau)F = 0, \tag{5.28}$$

where

$$N(\tau) = k^2\left(dk^2 + \frac{2d}{\tau} - \frac{2\alpha\mu}{\tau^2}\right), \quad D(\tau) = k^2(d+1) + \frac{2}{\tau}. \tag{5.29}$$

As noted, the last term in $N(\tau)$ is the only one in which the dimensionless parameter α (the grouping with the chemotaxis parameters) appears. The parameter μ appears explicitly only in that term as well but it is also contained in the expression for τ and so its effect is not so easily isolated. Note that $D(\tau)$ is positive for all $\tau > 0$, while $N(\tau)$ can be positive, negative or zero for τ near $\tau_0 = 1 + \mu$ (that is, where the dimensional time $t = 0$). For τ sufficiently large, $N(\tau) > 0$. Let us consider $N(\tau)$ and $D(\tau)$ to be constant for the moment, in which case the solution of (5.28), denoted by $\tilde{F}$, is formally

$$\tilde{F}(\tau) = L_1 e^{\lambda_+\tau} + L_2 e^{\lambda_-\tau}, \quad \lambda_\pm = \frac{1}{2}\left[-D(\tau) \pm \sqrt{D(\tau)^2 - 4N(\tau)}\right], \tag{5.30}$$

where the L's are constants of integration. Over a small interval of τ we can think of $N(\tau)$ and $D(\tau)$ to be approximately constant. Referring to the solution $\tilde{F}$, since $D(\tau) > 0\,\forall\,\tau$, we have $\mathrm{Re}\,(\lambda_-) < 0\,\forall\,\tau$. The sign of $\mathrm{Re}\,(\lambda_+)$, however, can vary depending on the sign of $N(\tau)$.

At this point, we are mainly interested in seeing how the chemotaxis coefficient α and the wavenumber k (or mode m) alter the solutions. Consider the effect of increasing α. If α is sufficiently large then $N(\tau)$ will be negative for small values of τ, including τ_0. As τ increases, $N(\tau)$ will increase through zero and become positive. The effect on λ_+ is to make the real part of the eigenvalue positive for small enough τ and negative for large τ. The point $\tau = \tau_{\text{crit}}$ at which λ_+ passes through zero is the same point at which $N(\tau)$ becomes zero. So, for small τ, one component of $\tilde{F}$ is a growing exponential, while for larger τ both exponentials are decaying. We predict therefore, that α has a destabilising influence; that is, the growth of pattern becomes more likely as α increases because it makes $N(\tau)$ more negative for $\tau < \tau_{\text{crit}}$. We could have predicted the destabilising effects of α, of course, from (5.20); it is the quantification of its destabilising influence that requires the analysis here.

Recall that the mode $m^2 = k^2 l^2/\pi^2$. For sufficiently large k^2, $N(\tau)$ in (5.29) becomes positive for all τ, resulting in solutions which are strictly decaying. This leads us to predict that the lowest frequency modes are the most unstable, and we would not expect to see modes of frequency larger than

$$K^2 = \frac{2}{d(1+\mu)}\left(\frac{\alpha\mu}{1+\mu} - d\right) \tag{5.31}$$

which is obtained by solving $N(\tau_0) = 0$. As time increases fewer and fewer modes remain unstable, and, as $\tau \to \infty$ the only unstable modes are those in a diminishing neighbourhood of 0. We can determine the fastest growing wavenumber, K_{grow} say, at any time by simply setting $\lambda(k^2) = 0 \equiv N(\tau) = 0$ and solving for k^2. This gives

$$K^2_{\text{grow}} = \frac{2}{\tau}\left(\frac{\alpha\mu}{d\tau} - 1\right).$$

If the approximation of constant coefficients in (5.28) is reasonably valid over small but finite intervals of τ, then a series of solutions $\tilde{F}$ computed in sequential intervals $\Delta\tau$ could give rise to a solution which increases to a maximum and then decreases for all τ afterwards. The increasing phase would occur while λ_+ is positive. When we computed a numerical solution of the equation it confirmed the expected behaviour; Figure 5.4 is one such simulation for the parameter values given there.

The true location $\tau = \tau_{\text{crit}}$ of the maximum value of $F(\tau)$, $F_{\max}$, may be close to $\tilde{\tau}_{\text{crit}}$, given analytically by

$$N(\tilde{\tau}_{\text{crit}}) = 0 \Leftrightarrow \tilde{\tau}_{\text{crit}} = \frac{1}{k^2}\left[-1 + \sqrt{1 + \frac{2\alpha\mu k^2}{D}}\right]. \tag{5.32}$$

Tyson et al. (1999) compared it with τ_{crit} obtained numerically: the comparison is very close and gets even better as the mode k^2 (proportional to m^2) and parameter α increase.

The difference between $\tilde{\tau}_{\text{crit}}$ and τ_{crit} gives an indication of the size of $d^2F/d\tau^2$ at τ_{crit}. By definition, τ_{crit} is the time at which $dF/d\tau = 0$ and so (5.28) reduces to

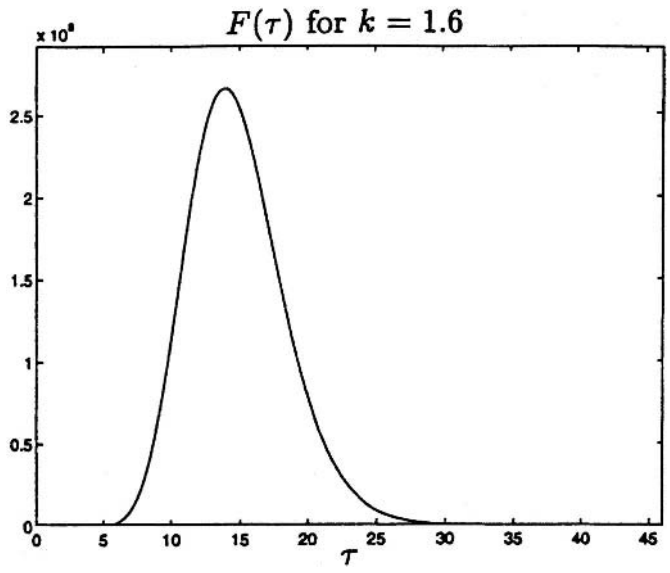

Figure 5.4. The amplitude F(τ) for the wavenumber $k = 1.6$ perturbation of the initial uniform cell density. From (5.24) and the parameters chosen this is equivalent to the mode $m = 5$. The other parameter values are: $d = 0.33$, $\alpha = 80$, $\mu = 1$, $u_0 = 1$, $w = 1$ and $l = 10$. (From Tyson 1996)

$$\left.\frac{d^2F}{d\tau^2}\right|_{\tau_{\text{crit}}} = -N(\tau_{\text{crit}})F.$$

Since the second derivative of a function is negative at a maximum we know that $N(\tau_{\text{crit}})$ is positive. Thus τ has already increased past the point where $N(\tau)$ changes sign, and $\tilde{\tau}_{\text{crit}}$ gives a minimum estimate for τ_{crit}. Since $\tilde{\tau}_{\text{crit}}$ and τ_{crit} are reasonably close, this suggests that $N(\tau_{\text{crit}})$ may be close to zero. In turn, this indicates that $d^2F/d\tau^2$ may be numerically small at the maximum, $F_{\max}$.

We are thus encouraged to solve (5.28) with the second derivative term omitted. After some straightforward algebra we get the solution of the resulting first-order ordinary differential equation as

$$F_1(\tau) = \left[\frac{(d+1)k^2\tau_0 + 2}{(d+1)k^2\tau + 2}\right]^{\alpha\mu k^2 - (2d(d-1)/(d+1)^2)} \left[\frac{\tau}{\tau_0}\right]^{\alpha\mu k^2} e^{[d/(d+1)]k^2(\tau_0 - \tau)}, \tag{5.33}$$

which satisfies $F(\tau_0) = 1 (= f(0))$. Plots of the first- and second-order equation solutions $F(\tau)$ and $F_1(\tau)$ are shown in Figures 5.5 and 5.6.

At first glance we notice the marked difference in the height of the two functions. Apart from this difference however, the two functions have many similarities. The peaks occur at approximately the same value of τ, and the peak interval, defined as the time

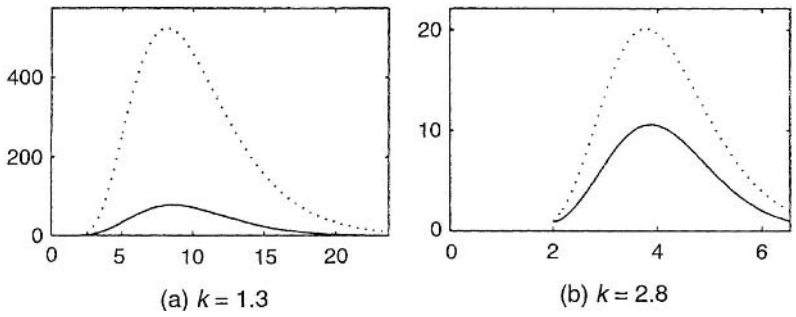

Figure 5.5. $F(\tau)$ (solid line) and $F_1(\tau)$ (dotted line) plotted together against τ for $\alpha = 30$ and wavenumbers: (**a**) $k = 1.3$, which corresponds to the mode $m = 4$, (**b**) $k = 2.8$, which corresponds to the mode $m = 9$. The parameter values are the same as in Figure 5.4. (From Tyson 1996)

during which $F(\tau) > F(\tau_0)$, is about the same, especially for the lower frequencies, and the two curves appear to be similarly skewed to the left. Increasing α results in a large increase in both $F_{\max}$ and $F_{1_{\max}}$. The two solutions are also similar with respect to the behaviour of the different modes investigated. The larger the value of k^2, the earlier τ_{crit} is reached, and the shorter the interval over which F or F_1 is larger than the initial value F_0.

If we normalise the data for $F(\tau)$ and $F_1(\tau)$ so that they lie in the interval [0, 1] we see in Figure 5.6 that the two solutions map almost directly on top of each other. So, the main difference between the approximate and numerical solutions is simply a scaling factor. This scaling factor is large, which suggests that the second-order derivative term is not small outside the neighbourhood of the maximum.

At this stage we have an intuitive understanding of the behaviour of the solutions $F(\tau)$ of (5.28). We also have an approximate analytic solution, $F_1(\tau)$ in (5.33), which we can use to predict the effect of changing various parameters.

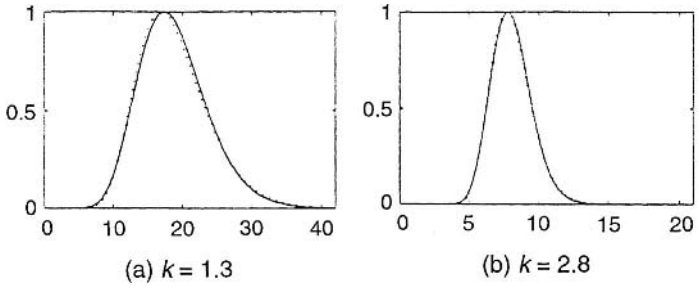

Figure 5.6. The solutions $F(\tau)$ (solid line) and $F_1(\tau)$ (dotted line) plotted against τ and normalised to lie between 0 and 1. (**a**) $k = 1.3$, which corresponds to the mode $m = 4$, (**b**) $k = 2.8$, which corresponds to the mode $m = 9$. The parameter values are the same as in Figure 5.4. (From Tyson 1996)

5.4 Interpretation of the Analytical Results and Numerical Solutions

We are particularly interested in the model's predictions as regards the number of aggregates which will form, and how long they will be visible, that is, when $F(\tau)$ is sufficiently large. If the nonlinear effects are not too strong, we should expect that the number of aggregates will be determined by the combined effect of the solutions corresponding to the various modes.

Some numerical results are shown in Figure 5.7. Note that there is one wavenumber (mode) which reaches a higher amplitude than any other. We refer to this wavenumber as $k_{\max}$; here $k_{\max} = 2.20$. Also note that every wavenumber k larger than $k_{\max}$, initially has a slightly higher growth rate than $k_{\max}$. These high frequencies quickly begin decaying, however, while the amplitude of the $k_{\max}$ pattern is still growing rapidly. We surmise that the $k_{\max}$ mode could be the first one to dominate the solution of the full nonlinear system of partial differential equations.

Once the $k_{\max}$ solution begins to decay, solutions corresponding to small wavenumbers become largest in decreasing order. The amplitude of each solution with $k < k_{\max}$ is always in the process of decaying, once it supersedes the next highest mode. Thus we should see a continuous decrease in wavenumber of the observed pattern as time t increases, accompanied by a decrease in amplitude. This corresponds to the biologically observed coalescing of aggregates and eventual dissipation of pattern. Note that for these figures the wavenumber with the maximum growth is $K_{\text{grow}} = 5.47$ and so

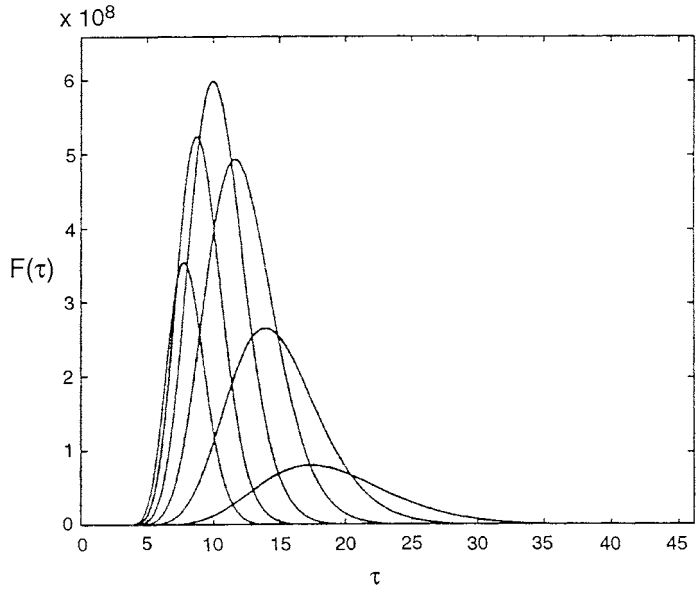

Figure 5.7. F(τ) for discrete values of $k = m\pi/l, m = 4$ to 9; that is, $k = 1.26$ to 2.83. The $m = 9$ curve decays the fastest, then the $m = 8$ curve, and so on. The curve corresponding to $m = 7$ has the highest peak. The parameter values are: $d = 0.33$, $\alpha = 80$, $\mu = 1$, $u_0 = 1$, $w = 1$ and $l = 10$. From (5.31) the maximum wavenumber $K = 10.9$. (From Tyson 1996)

$k_{\max}$ is less than K_{grow} by a factor of 2. For all of the numerical solutions observed by Tyson (1996) and Tyson et al. (1999) in this study $k_{\max}$ was consistently much less than K_{grow}.

One-Dimensional Numerical Simulation Results

We can now compare the predictions of the linear theory with the actual solution behaviour of the partial differential equations. Zero flux boundary conditions were used in all the simulations. The initial condition in chemoattractant concentration is zero everywhere on the domain, and in cell density it is a random perturbation about $u_0 = 1$. Among other numerical checks all of the solutions were checked against the integral form (5.35) of the conservation of bacteria since there is neither growth nor death in the liquid model.

A representative time sequence for $\alpha = 80$ is shown in Figure 5.8. The sequences were truncated at the time beyond which little change was observed in the number of peaks in cell density, and the pattern amplitude simply decreased. The plots in the left-hand column of each figure are the cell density profiles at various times τ, while the plots in the right-hand column are the corresponding power spectral densities. The density axes for the latter plots are restricted to lie above the mean value of the initial power spectral density, at $\tau = \tau_0$. This highlights the pattern modes which grow.

As predicted by (5.32), the power spectral density plots indicate that spatial patterns of modes higher than $K = 10.9$ do not grow. Also, the spread of 'nonzero' modes decreases as time increases. In the actual cell density distribution, the pattern observed initally has many peaks, and the number of these decreases over time. Our prediction that $k_{\max}$ is the spatial pattern mode which will dominate the solution is off by a factor of two in these figures. The mode which actually dominates the solution is $k_{\max} \approx 1.1$ while the predicted value is 2.2.

Two-Dimensional Numerical Simulation Results

In two dimensions we obtain the same sort of behaviour we found in the one-dimensional case. Again we started with an initial condition consisting of small random perturbations about a uniform distribution of cells and patterns consisting of a random arrangement of spots were generated as shown in Figure 5.8. The surface plot in Figure 5.9 clearly shows the comparative densities between the aggregates and the regions between them. The number of spots is large at first and then decreases over time as neighbouring aggregates coalesce. Eventually, all of the spots disappear.

Recall that this is exactly what is observed in the bacterial experiments. To begin with, bacteria are added to a petri dish containing a uniform concentration of succinate. The mixture is well stirred, and then allowed to rest. At this point, the state of the solution in the petri dish is mimicked by the initial condition for our model, namely, small perturbations of a uniform distribution of cells and succinate. After a short time, of the order of 20 minutes, the live bacteria aggregate into numerous small clumps which are very distinct from one another. This behaviour corresponds to the random arrangement of spots separated by regions of near zero cell density observed in the model solutions. Experimentally, the bacterial aggregates are seen to join together, forming fewer and larger clumps. This is also the situation in the mathematical model, and is particularly

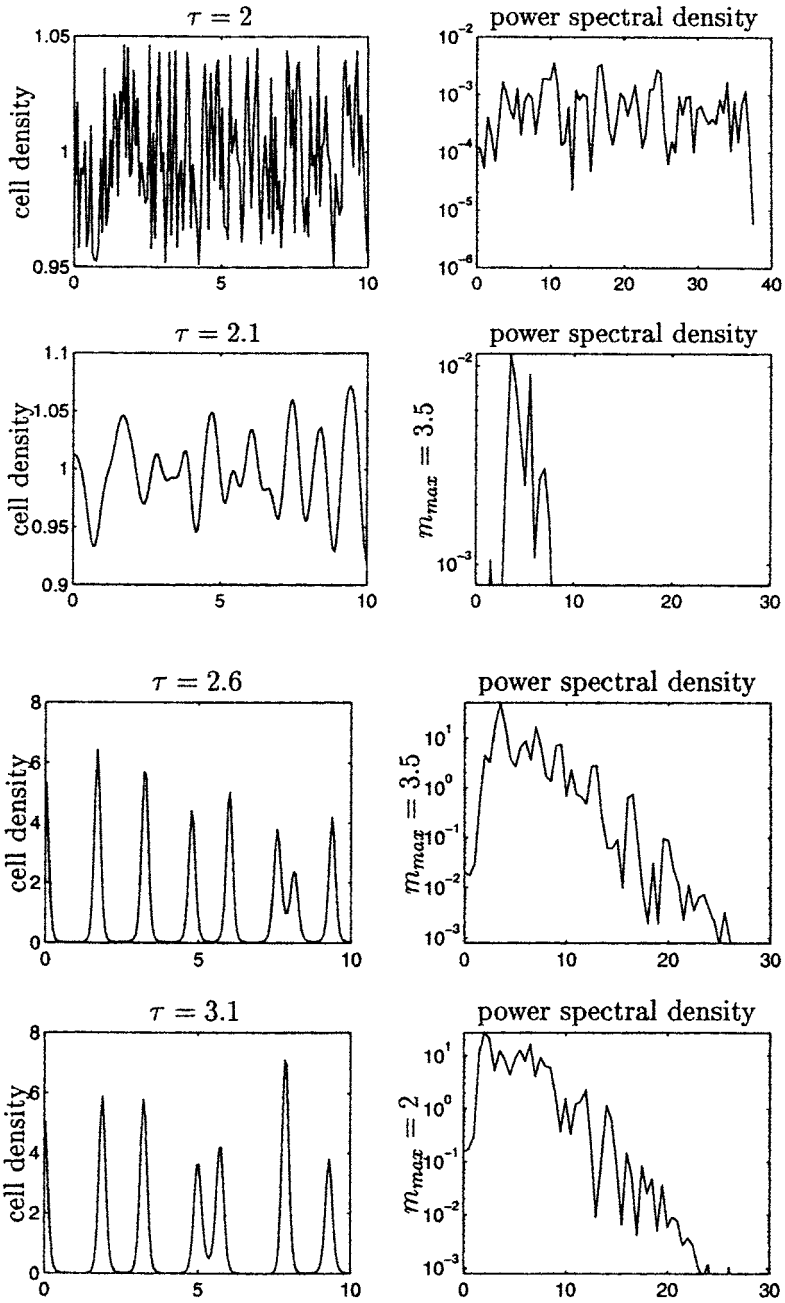

Figure 5.8. Numerical solution in one dimension of the liquid model system of equations (5.20) and (5.21). Left-hand plots show the bacterial cell density plotted against space at various times, τ. Right-hand plots show the corresponding power spectral density functions. Initially the cells are uniformly distributed over the one-dimensional domain and disturbed with a small perturbation of $O(0^{-1})$. Parameter values are the same as for Figure 5.7: $d = 0.33$, $\mu = 1$, $u_0 = 1$, $w_0 = 1$, $l = 10$ and $\alpha = 80$. (From Tyson 1996)

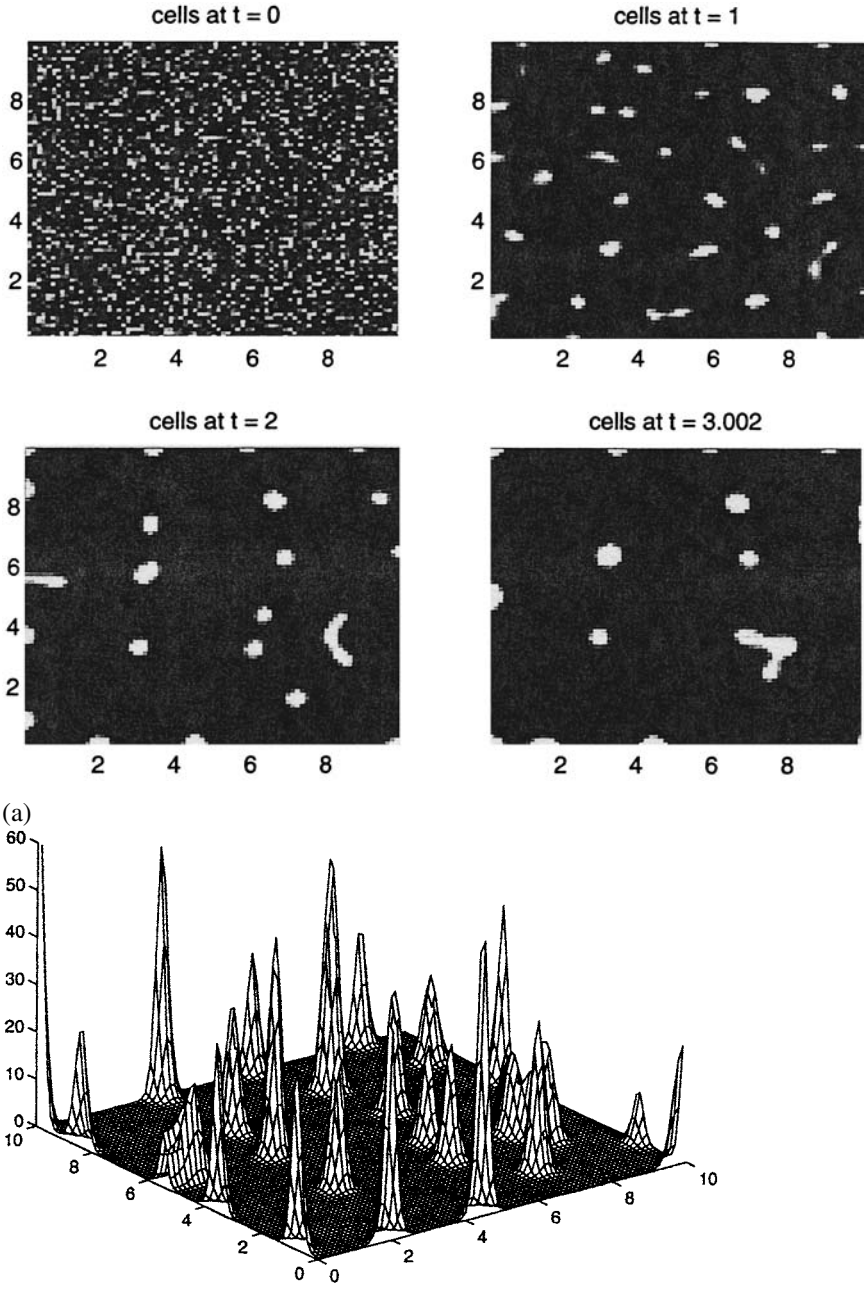

Figure 5.9. (**a**) Time evolution of two-dimensional cell density patterns arising from a uniform distribution of stimulant on a square domain. White corresponds to high cell density and black to low cell density. $\tau = 0$, the initial conditions, $\tau = 1$, $\tau = 2$, $\tau = 3.002$. (**b**) Surface plot of the solution for $\tau = 2$ showing the high density of the aggregates and the low density between them. Parameter values: $d_u = 0.33$, $\alpha = 80$, $\mu = 1$, $u_0 = 1$, $w = 1$ and $l = 10$. (From Tyson 1996)

clearly seen when the solutions are displayed as a movie with the frames separated by small time increments. In both the model and experiment, the spots eventually disappear and cannot be induced to re-form. This is again explained by the mathematical model as a saturation of the chemotactic response, which no longer has any effect as the production of chemoattractant increases continually.

Nonuniform Distribution of Stimulant

Up to now we have considered the cell density patterns which emerge in response to a spatially uniform distribution of the stimulant w; the above analysis qualitatively captures the experimentally observed behaviour in this case. Other patterns however, have been observed in experiment when the stimulant is added to the medium as a localised drop as we mentioned. If the model is essentially correct, it should also reproduce these patterns. This we briefly examine here.

With a nonuniform distribution of stimulant, we have to include diffusion of stimulant in the model. So, the model, given by equations (5.20) and (5.21), has to be expanded to include the equation for stimulant, namely, the system (5.14)–(5.16) in dimensionless form. This more general model is therefore

$$\frac{\partial u}{\partial t} = d\nabla^2 u - \alpha\nabla\cdot\left[\frac{u}{(1+v)^2}\nabla v\right] \tag{5.34}$$

$$\frac{\partial v}{\partial t} = \nabla^2 v + w\frac{u^2}{\mu + u^2} \tag{5.35}$$

$$\frac{\partial w}{\partial t} = d_s\nabla^2 w, \tag{5.36}$$

where the dimensionless $d_s = D_s/D_c$ (cf. (5.19)). With this formulation, we now require that the average value of $u(\mathbf{x}, t)$ and $w(\mathbf{x}, t)$ at all times be equal to 1.

Numerical results from a simulation of this model are shown in Figure 5.10. As observed experimentally in Figure 5.1, a ring of high cell density develops around the point where the stimulant was added. Some aggregates form inside the ring (also observed experimentally in Figure 5.1), but these are nowhere near as dense as the ring. The reason for this is that the ring recruits cells from outside its circumference, and so the number of cells available to it is much larger than that available to the aggregates in the centre.

Over time, simulations indicate that the radius of the ring decreases. Eventually the radius becomes so small that the ring is essentially one spot. It would be interesting to see if this behaviour is observed experimentally.

Before discussing the modelling of the more complex patterns in the semi-solid experiments it is perhaps helpful to recap what we have done in the above sections. We showed how a relatively simple but intuitively revealing analysis explains how evolving patterns of randomly or circularly arranged spots appear transiently in the chemotaxis model for the experimental arrangement. The central idea is to consider the rate of growth of individual modes over small time intervals, and extrapolate from this to the combined behaviour of all disturbance frequencies. Low mode number perturbations to

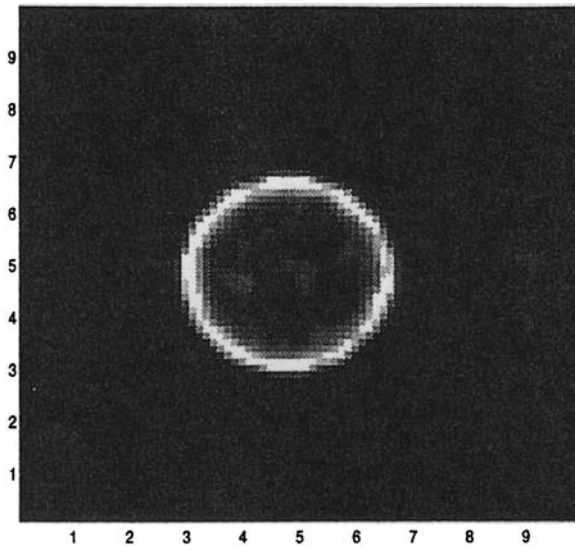

Figure 5.10. Two-dimensional cell density pattern arising from a nonuniform distribution of stimulant on a square domain. The stimulant was added as a single-humped function at the centre of the domain. Parameter values are the same as for Figure 5.9. (From Tyson 1996)

the uniform solution are unstable and grow in magnitude, but eventually these stabilize and decay with the larger mode numbers stabilizing first. This not only agrees qualitatively but also to a considerable extent quantitatively, with what is observed experimentally and numerically: clumps form, coalesce into larger aggregates and eventually disappear.

5.5 Semi-Solid Phase Model Mechanism for *S. typhimurium*

As we discussed in Section 5.1 in the semi-solid experiments, Budrene and Berg (1991) observed two very different pattern forming mechanisms. With *S. typhimurium* a thin bacterial lawn spreads out from the inoculum, and rings of more concentrated bacteria form well behind the lawn edge. Each ring may eventually break up into spots, but usually not until several more rings have formed at larger radii as shown in Figure 5.2. The second pattern forming mechanism is exhibited by *E. coli*, and involves first the formation of an expanding ring of high bacterial density, referred to as a swarm ring. As this swarm ring expands, it leaves behind smaller aggregates of bacteria, which form the striking patterns shown in Figure 5.3.

The bacterial lawn well ahead of the *S. typhimurium* pattern suggests that a spatially and temporally uniform steady state is first established, and then the pattern forms on it. As we showed, the model for the semi-solid experiments has no nonzero steady state. If consumption of nutrient is sufficiently slow, however, we can neglect it and the model reduces to two equations which admit the necessary steady state. We suppose then, that in the first pattern formation mechanism, consumption of nutrient is negligible.

This assumption is further supported by the fact that, experimentally, food is present in quantities well above the saturation level for the cells.

The second patterning mechanism appears to involve a vigorous nutrient consumption rate (Budrene and Berg 1995). There is little left behind the expanding swarm ring. In this case, all three equations of the semi-solid model are important.

We start by nondimensionalising the model system of equations (5.11)–(5.13) for the semi-solid experiments by setting

$$\begin{aligned} &u = \frac{n}{n_0}, \quad v = \frac{c}{k_2}, \quad w = \frac{s}{\sqrt{k_9}}, \quad t^* = k_7 n_0 t, \quad \nabla^{*2} = \frac{D_c}{k_7 n_0}\nabla^2, \\ &d_u = \frac{D_n}{D_c}, \quad d_w = \frac{D_s}{D_c}, \quad \alpha = \frac{k_1}{D_c k_2}, \quad \rho = \frac{k_3}{k_7}, \quad \delta = \frac{k_4}{n_0}, \\ &\beta = k_5 \frac{\sqrt{k_9}}{k_7 k_2 n_0}, \quad \kappa = \frac{k_8}{k_7\sqrt{k_9}}, \quad \mu = \frac{k_6}{n_0^2} \end{aligned} \tag{5.37}$$

and we obtain the dimensionless model, (with parameter estimates given in Table 5.3) where for algebraic convenience we have omitted the asterisks,

$$\frac{\partial u}{\partial t} = d_u \nabla^2 u - \alpha \nabla \cdot \left[\frac{u}{(1+v)^2} \nabla v \right] + \rho u \left(\delta \frac{w^2}{1+w^2} - u \right) \tag{5.38}$$

$$\frac{\partial v}{\partial t} = \nabla^2 v + \beta w \frac{u^2}{\mu + u^2} - uv \tag{5.39}$$

$$\frac{\partial w}{\partial t} = d_w \nabla^2 w - \kappa u \frac{w^2}{1+w^2}. \tag{5.40}$$

Recall that in the *S. typhimurium* experiments there are two distinct steps in the pattern forming process in the first of which there is a thin, disk-shaped bacterial lawn, suggesting that a spatially and temporally uniform steady state is temporarily present. During the second step a high density cluster of bacteria forms in the shape of a ring which appears well behind the leading edge of the bacterial lawn, suggesting that the ring pattern forms on top of the intermediate steady state. Since pattern is still forming long after the lawn has been established, consumption of nutrient in the lawn must be

Table 5.3. Known dimensionless parameter values calculated from the dimensional parameter values listed in Table 5.1.

Parameter	Value
d_u	0.2–0.5
d_w	0.8–1.0
α	87
δ	3.5

negligible. So, we can approximate the full system by neglecting the dynamics of food consumption. Also, since the concentration of nutrient is large, but the concentration of cells is small, we can study the simplified two-equation model

$$\frac{\partial u}{\partial t} = d_u \nabla^2 u - \alpha \nabla \cdot \left[\frac{u}{(1+v)^2} \nabla v \right] + \rho u \left(\delta \frac{w}{1+w} - u \right) \tag{5.41}$$

$$\frac{\partial v}{\partial t} = \nabla^2 v + \beta w \frac{u^2}{\mu + u^2} - uv. \tag{5.42}$$

The analysis of these equations is much easier than the analysis in Section 5.3 in that there is a homogeneous steady state in which both u and v are nonzero. So, we can use the usual linear analysis to determine whether or not this steady state is unstable and whether or not spatial patterns are likely to form. We also carried out a thorough nonlinear analysis some of whose results we discuss below since they are highly relevant to the specific patterns that are formed.

5.6 Linear Analysis of the Basic Semi-Solid Model

The linear analysis is the same as we discussed at length in Chapter 2 and is now straightforward. We linearize (5.41) and (5.42) about the nonzero steady state (u^*, v^*) given by

$$(u^*, v^*) = \left(\delta \frac{w}{1+w}, \beta w \frac{u^*}{\mu + u^{*2}} \right). \tag{5.43}$$

It is algebraically simpler in what follows to use general forms for the terms in the model equations (5.41) and (5.42): w is in effect another parameter here. We thus consider

$$\frac{\partial u}{\partial t} = d_u \nabla^2 u - \alpha \nabla \cdot [u \chi(v) \nabla v] + f(u, v) \tag{5.44}$$

$$\frac{\partial v}{\partial t} = d_v \nabla^2 v + g(u, v), \tag{5.45}$$

which on comparison with (5.41) and (5.42) define

$$\chi(v) = \frac{1}{(1+v)^2}, \quad f(u, v) = \rho u \left(\delta \frac{w}{1+w} - u \right),$$

$$g(u, v) = \beta w \frac{u^2}{\mu + u^2} - uv. \tag{5.46}$$

We now linearise the system about the steady state in the usual way by setting

$$u = u^* + \varepsilon u_1, \quad v = v^* + \varepsilon v_1, \tag{5.47}$$

where $0 < \varepsilon \ll 1$. Substituting these into (5.44) and (5.45) we get the linearized equations

$$\frac{\partial u_1}{\partial t} = d_u \nabla^2 u_1 - \alpha u^* \chi^* \nabla^2 v_1 + f_u^* u_1 + f_v^* v_1 \tag{5.48}$$

$$\frac{\partial v_1}{\partial t} = d_v \nabla^2 v_1 + g_u^* u_1 + g_v^* v_1 \tag{5.49}$$

since $f^* = 0$ and $g^* = 0$. Here the superscript * denotes evaluation at the steady state. We write the linear system in the vector form

$$\frac{\partial}{\partial t}\begin{pmatrix} u_1 \\ v_1 \end{pmatrix} = (A + D\nabla^2)\begin{pmatrix} u_1 \\ v_1 \end{pmatrix}, \tag{5.50}$$

where the matrices A and D are defined by

$$A = \begin{bmatrix} f_u^* & f_v^* \\ g_u^* & g_v^* \end{bmatrix}, \quad D = \begin{bmatrix} d_u & -\alpha u^* \chi^* \\ 0 & d_v \end{bmatrix}. \tag{5.51}$$

We now look for solutions in the usual way by setting

$$\begin{pmatrix} u_1 \\ v_1 \end{pmatrix} = \begin{pmatrix} c_1 \\ c_2 \end{pmatrix} e^{\lambda t + i\mathbf{k}x}, \tag{5.52}$$

where $\mathbf{k}$ is the wavevector, the c's constants and the dispersion relation $\lambda(\mathbf{k})$, giving the growth rate, is to be determined. Substituting this into the matrix equation gives

$$\left[\lambda I + D|\,\mathbf{k}\,|^2 - A\right]\begin{bmatrix} u_1 \\ v_1 \end{bmatrix} = \begin{bmatrix} 0 \\ 0 \end{bmatrix},$$

which has nontrivial solutions if and only if the determinant of the coefficient matrix, $|\,\lambda I + D|\,\mathbf{k}|^2 - A\,| = 0$ (recall Chapter 2). So, the dispersion relation $\lambda(k^2)$, $k^2 = |\,\mathbf{k}\,|^2$ is given by the characteristic equation

$$\lambda^2 + \lambda\left[(d_u + d_v)k^2 - (f_u^* + g_v^*)\right] + \left[d_u d_v k^4 - (d_u g_v^* + d_v f_u^* + \alpha u^* \chi^* g_u^*)k^2 + f_u^* g_v^* - f_v^* g_u^*\right] = 0$$

with solutions denoted by λ^+ and λ^-.

We are interested in determining pattern modes which have at least one positive growth rate; that is, at least one solution has $Rl\lambda > 0$ so we focus on the larger of the two solutions, λ^+, given by

$$\lambda^+ = \tfrac{1}{2}\left[-b(k^2) + \sqrt{[b(k^2)]^2 - 4c(k^2)}\right], \tag{5.53}$$

where

$$b(k^2) = (d_u + d_v)k^2 - (f_u^* + g_v^*)$$
$$c(k^2) = d_u d_v k^4 - (d_u g_v^* + d_v f_u^* + \alpha u^* \chi^* g_u^*)k^2 + f_u^* g_v^* - f_v^* g_u^*. \quad (5.54)$$

Recalling the discussion in Chapter 2, if $Rl\lambda^+$ is positive (negative) then perturbations about the steady state will grow (decay). We look for solutions which are stable ($\lambda^+ < 0$) to purely temporal perturbations (that is, $k^2 = 0$), but unstable ($\lambda^+ > 0$) to at least one spatial mode, which is just like the pure diffusionally driven instability situation for some nonzero k_1 and k_2. Mathematically, we look for a range of parameters such that

$$\lambda^+(0) < 0, \quad \lambda^+(k^2) > 0 \text{ for all } k \text{ such that } 0 \leq k_1^2 < k^2 < k_2^2. \quad (5.55)$$

To satisfy the first of (5.55) we must have

$$b(0) = f_u^* + g_v^* < 0, \quad c(0) = f_u^* g_v^* - f_v^* g_u^* > 0. \quad (5.56)$$

Note that these conditions imply that λ^- is always negative so we need only focus on λ^+. Graphically, these conditions yield an inverted parabolic curve for $\lambda(k^2)$, which has its maximum to the right of $k^2 = 0$ and so is the most basic dispersion relation which gives diffusion-chemotaxis-driven instability discussed in detail in Chapter 2. Typical dispersion relations are shown in Figure 5.11, where by way of example we have shown how they vary with the parameter μ: for μ small enough there is no range k_1^2, k_2^2.

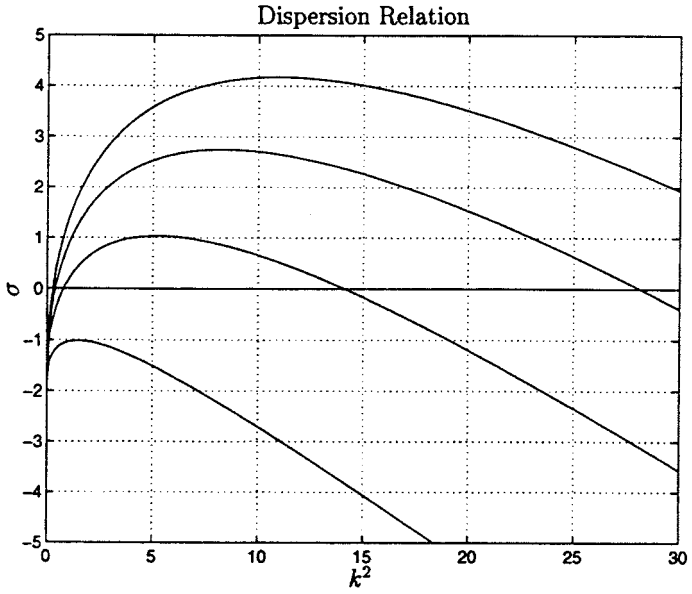

Figure 5.11. The dispersion relation, $\lambda(k^2)$ for parameter values $d_v = 1.0$, $d_u = 0.3$, $\alpha = 80$, $\beta = 2$, $\mu = 4$, 6, 8 and 10, $\delta = 2$, $\rho = 1$ and $w = 10$. The curve corresponding to $\mu = 4$ is the lowest one.

We are interested in the intersection of the curve with $\lambda = 0$ which gives k_1^2 and k_2^2. These correspond to a boundary in parameter space, which from (5.54) is given by the two solutions k^2 of

$$d_u d_v k^4 - (d_u g_v^* + d_v f_u^* + \alpha u^* \chi^* g_u^*) k^2 + f_u^* g_v^* - f_v^* g_u^* = 0. \tag{5.57}$$

In general, for each set of parameter values there are two, one or zero values of k^2 which satisfy (5.57). At bifurcation, where there is one value, we have

$$k_c^2 = \frac{d_u g_v^* + d_v f_u^* + \alpha u^* \chi^* g_u^*}{2 d_u d_v} \tag{5.58}$$

and

$$(d_u g_v^* + d_v f_u^* + \alpha u^* \chi^* g_u^*)^2 - 4 d_u d_v (f_u^* g_v^* - f_v^* g_u^*) = 0, \tag{5.59}$$

where k_c is the critical wavenumber. Solving the last equation for α and substituting it into (5.58) we get the crucial values

$$\alpha = \frac{-(d_u g_v^* + d_v f_u^*) + 2\sqrt{d_u d_v (g_v^* f_u^* - g_u^* f_v^*)}}{u^* \chi^* g_u^*}, \quad k_c^2 = \sqrt{\frac{(f_u^* g_v^* - f_v^* g_u^*)}{d_u d_v}}, \tag{5.60}$$

which give the parameter spaces for diffusion-chemotaxis-driven spatial instability in terms of the other parameters in the model system via the functions χ, f and g, here defined by (5.46), and their derivatives evaluated at the steady state.

For these results the positive solutions to the quadratic were chosen. Equation (5.60) defines a critical boundary set in parameter space which separates the two regions of positive and negative λ. The curve (5.59) is the bifurcation where $\lambda^+ = 0$ and wave patterns will neither grow nor decay. A sequence of these curves is shown in Figure 5.12 for various values of μ. On the upper side of each curve, $\lambda^+ > 0$ and all unstable pattern modes will grow, that is, for all $k_1^2 < k^2 < k_2^2$ obtained from (5.57). We do not know at this point what patterns to expect, only that spatial patterns are possible. To go further and determine which patterns will emerge is a nonlinear problem. To date the only analytical way to determine these is by what is called a weakly nonlinear analysis which means an anlysis near where the solutions bifurcate from spatial homogeneity to spatial heterogeneity. Some of the references where this has been done for reaction diffusion equations were given in Chapter 2. Exactly the same procedures are used in these types of equations but are just a little more complex. Zhu and Murray (1995) carried out a nonlinear analysis and evaluated, analytically, the parameter spaces for both reaction diffusion and diffusion-chemotaxis systems to compare their potential for generating spatial pattern. As already mentioned, Tyson (1996) used the method to analyze the specific model equations we have discussed here.

We do not carry out the (rather complicated) nonlinear analysis here (refer to Zhu and Murray 1995 and Tyson 1996 for a full discussion). Here we just sketch the proce-

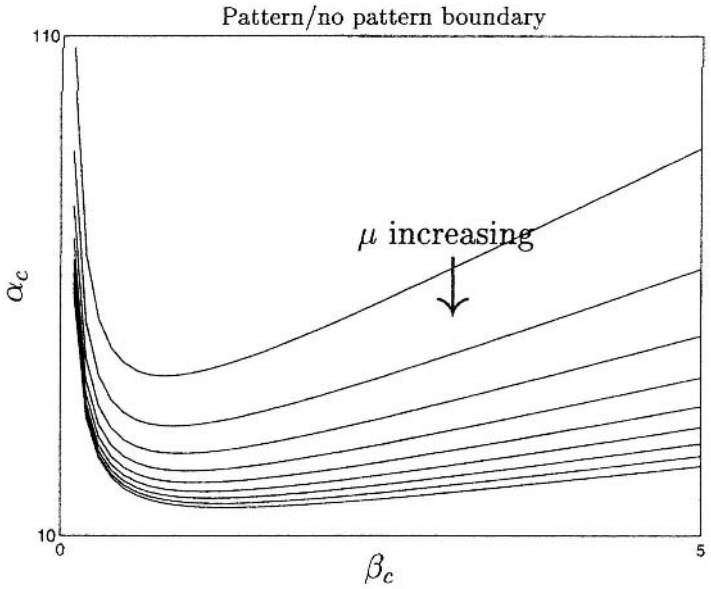

Figure 5.12. The boundary in (α_c, β_c) parameter space between regions where patterns are possible and where they are not. For (α, β) pairs above each line patterns are possible ($\lambda > 0$) while below, they are not. The parameter values are $d_{uc} = 0.3$, $d_{vc} = 1.0$, $\mu_c = 4$ (uppermost line), to 8 (lowermost line) in steps of 0.5, $\delta_c = 2$, $\rho_c = 0.5$ and $w_c = 5$. (From Tyson 1996)

dure and give the results. From the linear analysis we first determine in what parameter regions patterns are possible. The nonlinear analysis gives, in effect, the type of patterns which will form. The analysis is based on the assumption that the parameters are such that we are close to the bifurcation curve in parameter space. We develop an asymptotic analysis based on one parameter (the one of specific interest), for example, the chemotaxis parameter α, which is close to its bifurcation value, α_c, on the bifurcation curve but whose value moves the system into the pattern formation space as it passes through its critical value. We start with the linear solution to the boundary value problem; for example, in one dimension it involves a solution including $e^{\lambda(t)} \cos kx$, where k is in the unstable range of wavenumbers. On a linear basis this solution will start to grow exponentially with time with a growth rate $e^{\lambda(k)t}$ with $\lambda(k)$ the dispersion relation. Intuitively, by examining the undifferentiated terms in the system of equations (5.38)–(5.40), the solutions can not grow unboundedly. In a weakly nonlinear analysis we first consider the linear solution to be the solution to the linear boundary value problem with $k^2 = k_c^2$; that is, the parameters are such that we are close to the bifurcation curve from no pattern to pattern. An asymptotic perturbation method is then used to study the solutions in the form where the magnitude (or amplitude) of the solution is a slowly varying function of time. The conditions under which the amplitude is bounded as $t \to \infty$ are determined. This procedure then determines which of the various solution possibilities will evolve as stable solutions. We give a few more details to further explain the general procedure when we discuss the forms of the possible linear solutions to the boundary value problem.

Linear Boundary Value Problem

A necessary prerequisite for the nonlinear analysis is solving the linear boundary value problem relevant to the nonlinear analysis. The pattern types which are possible depend on the number of different wavevectors **k** allowed by the boundary conditions. From our point of view we are interested in having the experimental domain tesselated by repeating patterns. In the numerical simulations a square domain was chosen for numerical simplicity and so we are interested in square or rectangular tiles giving stripes and spots. So, each square or rectangular unit is subject to periodic boundary conditions. In general, with regular tesselations, we can have squares, stripes, hexagons, and so on as we discussed in Chapter 2.

Consider the rectangular domain, S, defined by $0 \leq x \leq l_x, 0 \leq y \leq l_y$ with the sides denoted by $S_1{:}x = 0, 0 \leq y \leq l_y$, $S_2{:}x = l_x, 0 \leq y \leq l_y$, $S_3{:}y = 0, 0 \leq x \leq l_x$, $S_4{:}y = l_y, 0 \leq x \leq l_x$. The spatial eigenvalue problem with periodic boundary conditions is then

$$\nabla^2\psi + k^2\psi = 0, \qquad \begin{cases} \psi|_{S_2} = \psi|_{S_4} \\ \psi|_{S_1} = \psi|_{S_3} \end{cases}. \tag{5.61}$$

The possible eigensolutions of the partial differential equation (5.61) are

$$\psi = \mathrm{A}\cos(\mathbf{k}_n \cdot \mathbf{x}) + \mathrm{B}\sin(\mathbf{k}_n \cdot \mathbf{x}), \tag{5.62}$$

where the $\mathbf{k}_n^2$ are allowable eigenvectors, which we discuss below. Substituting the boundary conditions in (5.61) into the solutions (5.62) we obtain

$$\begin{cases} \cos(\mathbf{k}_n \cdot (0, y)) = \cos(\mathbf{k}_n \cdot (l_x, y)) \\ \sin(\mathbf{k}_n \cdot (x, 0)) = \cos(\mathbf{k}_n \cdot (x, l_x)) \\ \cos(\mathbf{k}_n \cdot (0, y)) = \cos(\mathbf{k}_n \cdot (l_y, y)) \\ \sin(\mathbf{k}_n \cdot (x, 0)) = \cos(\mathbf{k}_n \cdot (x, l_y)) \end{cases}$$

which after using some trigonometric identities can be written as

$$\begin{cases} \cos(k_n^y y)\left[1 - \cos(k_n^x l_x)\right] + \sin(k_n^y y)\sin(k_n^x l_x) = 0 \\ \sin(k_n^y y)\left[1 - \cos(k_n^x l_x)\right] - \cos(k_n^y y)\sin(k_n^x l_x) = 0 \\ \cos(k_n^x x)\left[1 - \cos(k_n^y l_y)\right] + \sin(k_n^x x)\sin(k_n^y l_y) = 0 \\ \sin(k_n^x x)\left[1 - \cos(k_n^y l_y)\right] - \cos(k_n^x x)\sin(k_n^y l_y) = 0, \end{cases} \tag{5.63}$$

where $\mathbf{k}_n^T = (k_n^x, k_n^y)$. The general solutions of (5.63) are

$$\mathbf{k}_1 = \begin{bmatrix} 0 \\ 2m\pi/l_y \end{bmatrix}, \quad \mathbf{k}_2 = \begin{bmatrix} 2n\pi/l_x \\ 0 \end{bmatrix}, \quad \mathbf{k}_3 = \begin{bmatrix} 2p\pi/l_x \\ 2q\pi/l_y \end{bmatrix},$$

where m, n, p and q are all integers.

We are concerned with parameters such that we are near the bifurcation curve so we are particularly interested in the solutions $\mathbf{k}_n$ which satisfy $|\,\mathbf{k}_n\,|^2 = k_c^2$.

The number of such solution vectors which equations (5.63) admit depends on the relationship between l_x and l_y. Suppose $k_c^2 = (2M\pi/l)^2$ and also that S is square with sides $l_x = l_y = l$. If $M = 1$ then there are two possible solution vectors:

$$\mathbf{k}_1 = \begin{bmatrix} 0 \\ 2\pi/l \end{bmatrix}, \quad \mathbf{k}_2 = \begin{bmatrix} 2\pi/l \\ 0 \end{bmatrix}. \tag{5.64}$$

If $M = 5$ then there are four possible solution vectors:

$$\begin{aligned} \mathbf{k}_1 &= \begin{bmatrix} 0 \\ 2 \cdot 5\pi/l \end{bmatrix}, \quad \mathbf{k}_2 = \begin{bmatrix} 2 \cdot 5\pi/l \\ 0 \end{bmatrix} \\ \mathbf{k}_3 &= \begin{bmatrix} 2 \cdot 3\pi/l \\ 2 \cdot 4\pi/l \end{bmatrix}, \quad \mathbf{k}_4 = \begin{bmatrix} 2 \cdot 4\pi/l \\ 2 \cdot 3\pi/l \end{bmatrix}. \end{aligned} \tag{5.65}$$

These solution vectors are important in the nonlinear analysis.

5.7 Brief Outline and Results of the Nonlinear Analysis

With the linear analysis we can only determine the small amplitude initial behaviour of u and v about the uniform steady state when the steady state is driven unstable to spatially heterogenous perturbations. These spatially inhomogeneous solutions initially grow exponentially and are clearly not valid for all time. For the class of problems here we can carry out a nonlinear asymptotic analysis and obtain the solutions to $O(\varepsilon)$ (and in principle to higher orders but the algebra is prohibitive) which are valid for all time. As mentioned the details of the procedure are given by Zhu and Murray (1995) for several pattern formation mechanisms including a diffusion-chemotaxis one. For the more complex chemotaxis mechanism the analysis has been carried out by Tyson (1996). Here we sketch the analytical procedure, namely, a multi-scale asymptotic analysis, for determining small perturbation solutions valid for all time of the system of equations (5.41) and (5.42) the general forms of which are (5.44) and (5.45). We start by writing

$$\begin{aligned} u &= u^* + \hat{u} = u^* + (\varepsilon u_1 + \varepsilon^2 u_2 + \varepsilon^3 u_3 + \cdots) \\ v &= v^* + \hat{v} = v^* + (\varepsilon v_1 + \varepsilon^2 v_2 + \varepsilon^3 v_3 + \cdots), \end{aligned} \tag{5.66}$$

where (u^*, v^*) is the spatially homogeneous steady state which depends on the model parameters and which, as we saw in the last section, can be driven unstable as a parameter passes through the bifurcation value which results in spatially unstable solutions. We scale time by writing

$$T = \hat{\omega} t, \quad \text{where } \hat{\omega} = \varepsilon\omega_1 + \varepsilon^2\omega_2 + \cdots, \tag{5.67}$$

where the $\omega_i, i = 1, 2, \ldots$ have to be determined.

Consider equation (5.44). Substituting the expansions (5.66) and (5.67) into the individual terms, we get

$$\begin{aligned}
\frac{\partial u}{\partial t} &= \hat{\omega}\frac{\partial \hat{u}}{\partial T}, \quad \nabla^2 u = \nabla^2 \hat{u} \\
\alpha\nabla\cdot[u\chi(v)\nabla v] &= \alpha\nabla\cdot\left[(u^*+\hat{u})\left(\chi^* + \chi_v^*\hat{v} + \tfrac{1}{2}\chi_{vv}^*\hat{v}^2 + \cdots\right)\nabla\hat{v}\right] \\
&= u^*\chi^*\nabla^2\hat{v} + \left(u^*\chi^*\nabla\hat{v} + \chi^*\nabla\hat{u}\right)\cdot\nabla\hat{v} \\
&\quad + \left(u^*\tfrac{1}{2}\chi_{vv}^*\nabla(\hat{v}^2) + \chi_v^*\nabla(\hat{u}\hat{v})\right)\cdot\nabla\hat{v} + \cdots \\
f(u,v) &= f^* + (f_u^* + f_v^*)\hat{u} + \tfrac{1}{2}(f_{uu}^* + f_{vv}^*)\hat{u}^2 + f_{uv}^*\hat{u}\hat{v} \\
&\quad + \tfrac{1}{6}(f_{uuu}^* + f_{vvv}^*)\hat{u}^3 + \cdots .
\end{aligned} \tag{5.68}$$

The first two expressions have linear terms in $\hat{u}$, while the last two expressions have linear, quadratic, cubic and so on with higher-order terms in $\hat{u}$ and $\hat{v}$; $f^* = 0$ by definition of the steady state. So (5.44) transforms into another equation with linear, quadratic and higher-order terms in $\hat{u}$ and $\hat{v}$. Equation (5.45) transforms in an equivalent way. In general then, (5.44) and (5.45) with (5.67) and (5.68) take the form

$$\hat{\omega}\frac{\partial}{\partial T}(\vec{\hat{u}}) = \left[D^*\nabla^2 + A^*\right]\vec{\hat{u}} + \mathcal{Q}^*(\vec{\hat{u}}) + \mathcal{C}^*(\vec{\hat{u}}) + \cdots, \quad \vec{\hat{u}} = \begin{bmatrix}\hat{u}\\ \hat{v}\end{bmatrix} \tag{5.69}$$

and where $*$ denotes evaluation at the steady state (u^*, v^*).

The quantities $A\vec{\hat{u}}$, $\mathcal{Q}(\vec{\hat{u}})$ and $\mathcal{C}(\vec{\hat{u}})$, represent the linear, quadratic and cubic terms respectively, of the expansion of the chemotaxis and reaction functions about the steady state. The matrices $A\vec{\hat{u}}$ and D were determined above in the linear analysis. We are interested in situations where the model parameters have particular values such that $\lambda = 0$. This occurs when the parameters are defined by (5.60); we call this set a critical parameter set. Basically, it means the parameter set is sitting on the boundary between growing spatially heterogeneous solutions and spatially homogeneous solutions.

If we now perturb one of the model parameters a, say, which can be any one of the parameters in (5.44) and (5.45), about its value in a critical set, the eigenvalue for temporal growth becomes

$$\begin{aligned}
\lambda(a) &= \lambda(a_c) + \left.\frac{\partial\lambda}{\partial a}\right|_{a_c}\Delta a_c + \cdots \\
&= \left.\frac{\partial\lambda}{\partial a}\right|_{a_c}\Delta a_c + \cdots
\end{aligned}$$

since $\lambda(a_c) = 0$ by definition of the critical parameter a_c. We take the perturbation to be such that

$$\left.\frac{\partial k_c^2}{\partial a}\right|_{a_c} = 0,$$

so that the perturbation effect on the solution $e^{\lambda t + i\vec{k}\cdot\vec{x}}$ is restricted to a change in the temporal growth rate λ. Then, if the change in a_c makes $\mathrm{Re}(\lambda(a))$ positive, the pattern mode corresponding to k_c^2 is predicted to grow according to linear theory. Depending on the parameters, the result can be a stable or unstable spatially heterogeneous solution. If this growth is sufficiently slow, we can predict whether or not it will develop into a temporally stable pattern and furthermore, what the characteristics of the pattern will be such as spots or stripes. We start by perturbing the steady state model (5.69) about the critical set. To keep the analysis simple we perturb only one parameter, and to keep the analysis general we call the parameter a. Tyson (1996) carried out the analysis with the actual parameters from the model equations and it is her results we give below.

Consider an expansion of the form

$$a = a_c + \hat{a} = a_c + (\varepsilon a_1 + \varepsilon^2 a_2 + \cdots). \tag{5.70}$$

Substituting this into (5.69) we get the system

$$\begin{aligned}\hat{\omega}\frac{\partial}{\partial T}(\vec{\hat{u}}) = &\left[D^{*c}\nabla^2 + A^{*c}\right]\vec{\hat{u}} + \mathcal{Q}^{*c}(\vec{\hat{u}}) + \mathcal{C}^{*c}(\vec{\hat{u}}) \\ &+ \hat{a}\left[D_a^{*c}\nabla^2 + A_a^{*c}\right]\vec{\hat{u}} + \hat{a}\,\mathcal{Q}_a^{*c}(\vec{\hat{u}}) \\ &+ \text{higher-order terms},\end{aligned} \tag{5.71}$$

where the superscript c denotes evaluation at the critical set. The change in the critical parameter a only occurs in $\hat{a}$ and so its effect can be isolated in the analysis.

Substituting the expansions for all of the small variables $\hat{()}$, and collecting and equating terms of like order in ε, we obtain systems of equations for each order in ε. For notational simplicity, the superscript c is omitted in the result, and for the remainder of the analysis all parameter values are from a critical set. To show what these equations look like we just give the $O(\varepsilon)$ and $O(\varepsilon^2)$ systems although to carry out the nonlinear analysis it is necessary to also have the $O(\varepsilon^3)$ system which is algebraically extremely complicated. We do not need them to sketch the procedure. The $O(\varepsilon)$ equations are

$$\begin{bmatrix}0\\0\end{bmatrix} = \begin{bmatrix} d_u\nabla^2 + f_u^* & -\alpha u^*\chi^*\nabla^2 + f_v^* \\ g_u^* & d_v\nabla^2 + g_v^*\end{bmatrix}\begin{bmatrix}u_1\\v_1\end{bmatrix} = L\begin{bmatrix}u_1\\v_1\end{bmatrix} \tag{5.72}$$

which are linear and define the coefficient matrix as the linear operator L. The order $O(\varepsilon^2)$ equations are

$$\begin{aligned}L\begin{bmatrix}u_2\\v_2\end{bmatrix} = &\omega_1\frac{\partial}{\partial T}\begin{bmatrix}u_1\\v_1\end{bmatrix} + \begin{bmatrix}\alpha(\chi^*\nabla u_1 + u^*\chi_v^*\nabla v_1)\cdot\nabla v_1\\ 0\end{bmatrix} \\ &- \begin{bmatrix}\frac{1}{2}f_{uu}^*u_1^2 + f_{uv}^*u_1v_1D + \frac{1}{2}f_{vv}^*v_1^2\\ \frac{1}{2}g_{uu}^*u_1^2 + g_{uv}^*u_1v_1 + \frac{1}{2}g_{vv}^*v_1^2\end{bmatrix} \\ &- a_1\begin{bmatrix}(f_u^*)_a & -(\alpha u^*\chi^*)_a\nabla^2 + (f_u^*)_a \\ (g_u^*)_a & (g_v^*)_a\end{bmatrix}\begin{bmatrix}u_1\\v_1\end{bmatrix}.\end{aligned} \tag{5.73}$$

The analysis, which needs the $O(\varepsilon^3)$ equations, requires the solutions of these linear systems of equations. This was done by Tyson (1996) (and an equivalent analysis by Zhu and Murray 1995). The algebra is horrendous but necessary to get the uniformly valid (for all time) solution to $O(\varepsilon)$ and to determine which specific patterns will be stable.

So as to be able to give the results and explain what the nonlinear analysis gives, we need the solutions to the $O(\varepsilon)$ system (5.72). To get them we look for solutions in the form

$$\begin{bmatrix} u_1 \\ v_1 \end{bmatrix} = \sum_{l=1}^{N} \vec{V}1_l A_l, \tag{5.74}$$

where

$$A_l = a_l(T)e^{i\vec{k}_l\cdot\vec{x}} + \bar{a}_l(T)e^{-i\vec{k}_l\cdot\vec{x}} \tag{5.75}$$

is the sinusoidal part of the solution. Relating this form to (5.62), $\bar{a}_l(T) + a_l(T) \propto B$. Substituting (5.74) into (5.72) we obtain an expression for $\vec{V}1_l$ to within an arbitrary constant multiple. This is usually chosen such that the magnitude of the vector is unity and so

$$\vec{V}1_l = \begin{bmatrix} V1_{l1} \\ V1_{l2} \end{bmatrix} = \frac{1}{\sqrt{(d_v|\vec{k}_l|^2 - g_v^*)^2 + (g_u^*)^2}} \begin{bmatrix} d_v|\vec{k}_l|^2 - g_v^* \\ g_u^* \end{bmatrix}. \tag{5.76}$$

Since we only consider critical sets of parameters, we know that $|\vec{k}_l|^2 = k_c^2 \forall l$ and so $\vec{V}1_l = \vec{V}1 \forall l$.

At this stage we do not know $a_l(T)$ and $\bar{a}_l(T)$, the complex amplitudes (which are functions of T the slowly varying time defined by (5.67)) of the $O(\varepsilon)$ solution; the solution amplitude is $|a_l(T)|$. The key to the nonlinear analysis is the determination of the amplitude. So, we have to solve the $O(\varepsilon^2)$ equations. Since these linear equations, with the same operator L, contain undifferentiated terms on the right-hand side it is possible to have solutions with secular terms, which are terms which involve expressions like $x \sin x$ which become unbounded for large x.

It is easy to see how secular terms arise if we consider the simple equation for $u(x)$:

$$u'' + u = -\varepsilon u',$$

where primes denote differentiation with respect to x, $0 < \varepsilon \ll 1$ and, to be specific, let us require $u(0) = 1, u'(0) = 0$. If we write $u = u_0 + \varepsilon u_1 + \cdots$ we assume all the $u_i, i = 1, 2, \ldots$ are all $O(1)$. Substituting this into the equation and collecting like terms in ϵ we get $u_0(x) = \cos x$ and the equation and boundary conditions for u_1, the $O(\varepsilon)$ terms, as

$$u_1'' + u_1 = \sin x, \quad u_1(0) = u_1'(0) = 0,$$

the solution of which is $u_1(x) = (1/2)(\sin x - x\cos x)$. So, $u_0 + \varepsilon u_1 + \cdots$ is not a uniformly valid solution since $u_1(x)$ is not $O(1)$ for all x because of the $x\cos x$ term: it is the secular term. The asymptotic procedure for obtaining uniformly valid solutions of this type of equation is pedagogically described in detail in the book on asymptotic analysis by Murray (1984).

To go back to the above discussion of the $O(\varepsilon^2)$ equations, it turns out that these do not give rise to secular terms and so the amplitude functions $a_l(T)$ and $\bar{a}_l(T)$ remain undetermined at this order. However, at $O(\varepsilon^3)$ secular terms do appear. It is at this stage that the equations for the amplitude are determined: they are chosen so that these secular terms do not occur in the $O(\varepsilon^3)$ solutions even though we do not actually find the solutions at this order. It is the algebra involved in obtaining these equations, known as the Landau equations, that is so complicated and detailed. The equations crucially involve the number N in (5.74) which is the number of modes in the solution which have $|k_l^2| = k_c^2$. We saw how the solutions and eigenvectors varied with this number in the discussion of the boundary value problem in the last section.

By way of example, let us suppose $N = 2$; then Tyson (1996) showed that the amplitude, or Landau, equations are

$$\frac{d|a_1|^2}{dT} = |a_1|^2(X_A|a_1|^2 + X_B|a_2|^2) + Y|a_1|^2 \tag{5.77}$$

$$\frac{d|a_2|^2}{dT} = |a_2|^2(X_B|a_1|^2 + X_A|a_2|^2) + Y|a_2|^2, \tag{5.78}$$

where the X_A, X_B and Y are complicated functions of the parameters of the original system (5.44) and (5.45) (and hence (5.41) and (5.42)). The $|a_1|$ and $|a_2|$ directly relate to the A and B in equation (5.62) except that here they are functions of time. Whether or not a stable spatially heterogeneous solution exists depends on the solutions of these amplitude equations as $t \to \infty$. They are just ordinary differential equations with constant coefficients. They have the following possible steady state solutions and their existence depends on the signs of the coefficients,

$$\begin{aligned}
&(1) \quad |a_1|^2 = 0, && |a_2|^2 = 0\\
&(2) \quad |a_1|^2 = 0, && |a_2|^2 = -\frac{Y}{X_A}\\
&(3) \quad |a_1|^2 = -\frac{Y}{X_A}, && |a_2|^2 = 0\\
&(4) \quad |a_1|^2 = -\frac{Y}{X_A + X_B}, && |a_2|^2 = -\frac{Y}{X_A + X_B}
\end{aligned} \qquad . \tag{5.79}$$

The first steady state corresponds to a zero amplitude pattern, or no pattern at all. The second and third correspond to a zero amplitude in one direction and a nonzero amplitude in the other, and this gives stripes. The fourth steady state has a nonzero amplitude in each direction and therefore gives spots. If none of these steady states is stable, then the analysis does not determine the type of pattern formed. This is referred to

Table 5.4. Conditions for stability of the patterns possible for the four steady states when the number of critical wavenumber vectors $\vec{k}_n$ is $N = 2$.

Steady State $(\mid a_1 \mid^2, \mid a_2 \mid^2)$	Pattern	Stability Conditions
(0,0)	none	$Y < 0$
$(0, -Y/X_A)$	horizontal stripes	$Y > 0$ $X_B/X_A > 1$
$(-Y/X_A, 0)$	vertical stripes	$Y > 0$ $X_B/X_A > 1$
$\left(-\frac{Y}{X_A + X_B}, -\frac{Y}{X_A + X_B}\right)$	spots	$Y > 0$ $X_A \pm X_B < 0$

as the undetermined region in the parameter plots which we show below. The conditions for stability of these steady states are summarized in Table 5.4. By computing X_A, X_B and Y over a given parameter space, we can use Table 5.4 to divide this space into regions where spots, stripes, no pattern or an undetermined pattern can occur. These parameter spaces were calculated by Tyson (1996) for the system under study here and by Zhu and Murray (1995) for a simpler reaction diffusion-chemotaxis system.

5.8 Simulation Results, Parameter Spaces and Basic Patterns

We present in this section some simulations of two models: equations (5.41) and (5.42) and a moderately simplified version. For these simulations we used initial conditions which strictly apply to the analysis. That is, the simulations are begun with a small (order ε) perturbation of the spatially and temporally unvarying steady state solution, and a smaller (order ε^2) perturbation of one of the parameters. Recall that the boundary conditions are periodic.

The Simplified Model

Consider first the following simplified model of (5.41) and (5.42),

$$\begin{aligned} \frac{\partial u}{\partial t} &= d_u \nabla^2 u - \alpha \nabla \left[\frac{u}{(1+v)^2} \nabla v \right] + \rho u(\delta - u) \\ \frac{\partial v}{\partial t} &= \nabla^2 v + \beta u^2 - uv. \end{aligned} \tag{5.80}$$

This model has only five parameters, and so the parameter space is a little easier to explore than for equations (5.41) and (5.42). If we take d_u and ρ to be fixed, then we can vary δ and β, and determine α from the first of (5.61). Each point in the δ, β plane will thus correspond to a critical set of parameters which we can use to determine X_A,

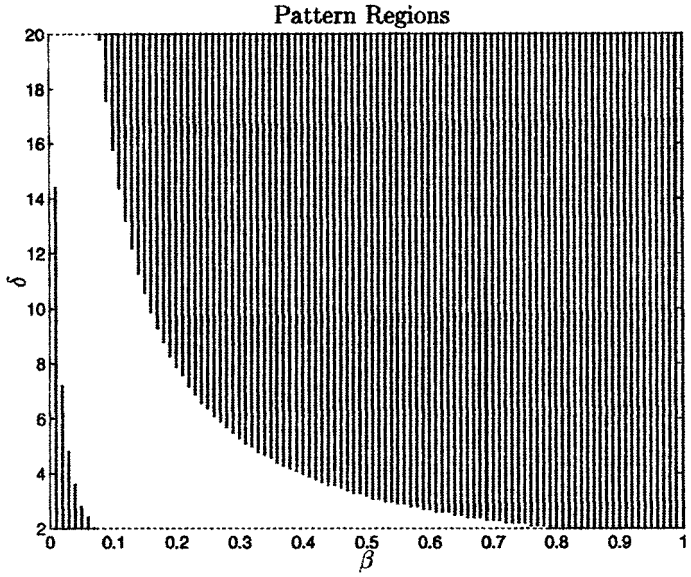

Figure 5.13. The pattern domain for the simple model (5.80) with $d_u = 0.25$, $\rho = 0.01$, $\mu = 1.0$ and $w_0 = 1.0$. As β is varied, the corresponding value of α is determined from equation (5.80). The perturbation parameter is β. The pattern regions based on the evaluated X_A, X_B and Y for Table 5.4 give stripes in the striped (dark) areas and spots in the clear (white) area. (From Tyson 1996)

X_B and Y. This approach creates the pattern regions shown in Figure 5.13. On this plot, curves of constant α are hyperbolas given by

$$\beta = \frac{(\sqrt{d_u} + \sqrt{\rho d_v})^2}{\alpha} \frac{(1+\delta)^2}{\delta}.$$

Numerical solutions were obtained for two sets of parameters: one from the upper stripes region, and one from the spots region. Simulations were performed on square domains just large enough to hold one full period of the pattern. This required the choice

$$l_x = l_y = \frac{2\pi}{\sqrt{k_c^2}}.$$

So, we expected to obtain one stripe for the stripe parameters and one spot for the spot parameters. These were found, and typical results for the cell density are shown in Figure 5.14. Each simulation has two plots which indicate the initial conditions and the steady state pattern.

Note that since the boundary conditions are periodic, the maximum of the spot or stripe pattern can occur anywhere in the domain. Also, for the stripe pattern, the orientation of the stripe is not determined from the analysis, since we are working with a square domain. So, for one set of random initial conditions the stripe will appear vertical, whereas for another set it will appear horizontal.

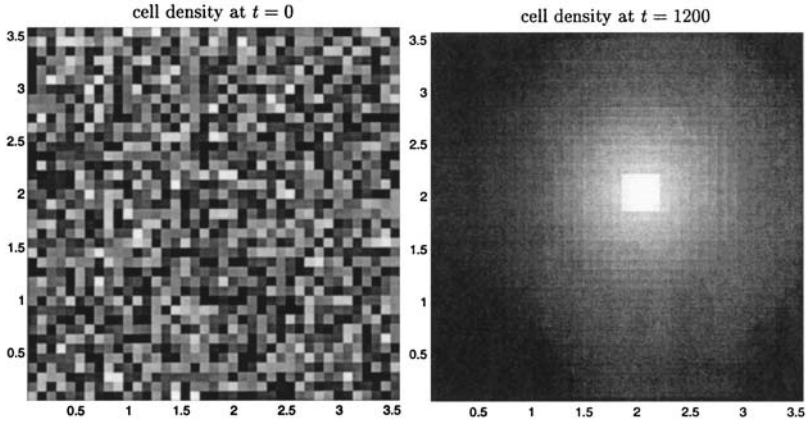

(a)

Figure 5.14. Simulation results from the simple model parameter domain where spots were predicted in Figure 5.13. Cell density is plotted as an image at $t = 0$ and at steady state. Cell density profiles are shown to demonstrate that the pattern has indeed reached a steady state, and the predicted cell density profile is also shown for comparison. The perturbation was $\varepsilon = 0.1$. The times given are in nondimensional units. White indicates high cell density, black the opposite. The parameter values are: (**a**) $d_u = 0.25$, $\alpha = 1.50$, $\beta = 0.1$, $\delta = 15.0$, $\rho = 0.01$, $w = 1.0$, $u_0 = u^* = 15.0$, $v_0 = v^* = 1.50$, $k_c^2 = 3.0$ and $l_x = l_y = l = 3.6276$ (domain which can sustain one 2π oscillation), a spot.

The Full Model

We consider now the more biologically accurate model

$$\begin{aligned}\frac{\partial u}{\partial t} &= d_u \nabla^2 u - \alpha \nabla \left[\frac{u}{(1+v)^2} \nabla^* v \right] + \rho u (\delta \frac{w^2}{1+w^2} - u) \\ \frac{\partial v}{\partial t} &= \nabla^2 v + \beta w \frac{u^2}{\mu + u^2} - uv, \end{aligned} \tag{5.81}$$

which has seven parameters, including w and for which we have experimental estimates for α, d_u and δ. One of the four remaining parameters can be determined from the bifurcation condition (5.58). In the simpler model we solved for the critical value of α given all of the other parameters. Since we know α, however, we would like to fix its value and solve for one of the unknown parameters. The simplest one to solve for is ρ, which is given by

$$\rho = \left[\frac{\sqrt{\alpha\beta\delta(\mu - \delta^2)}}{\mu + \delta(\beta + \delta)} - \sqrt{d_u} \right]^2 . \tag{5.82}$$

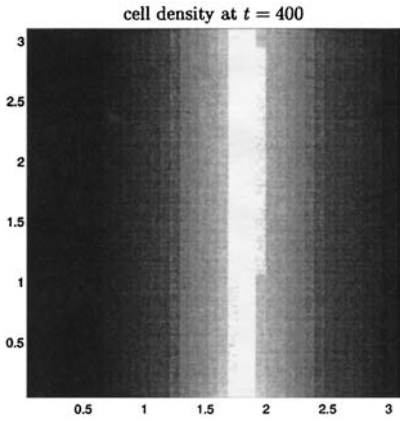

(b)

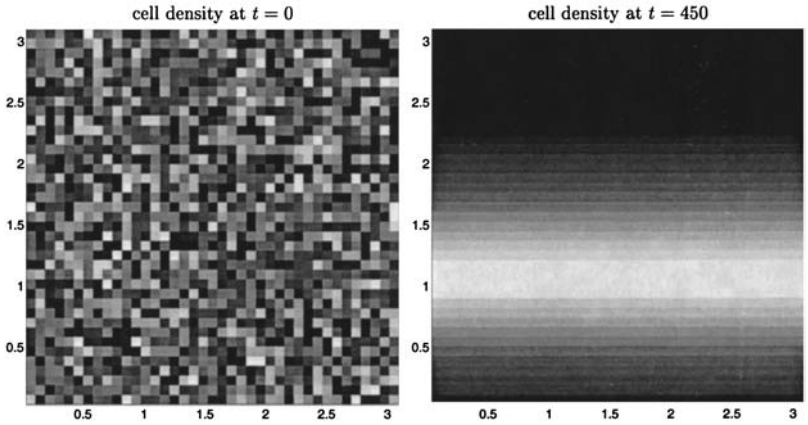

(c)

Figure 5.14. (continued) (**b**) and (**c**) $d_u = 0.25$, $\alpha = 2.25$, $\beta = 0.2$, $\delta = 20.0$, $\rho = 0.01$, $w = 1.0$, $u_0 = u^* = 20.0$, $v_0 = v^* = 4.0$, $k_c^2 = 4.0$ and $l_x = l_y = l = 3.1416$ (domain which can sustain one 2π oscillation) but a stripe. In (**a**) and (**b**) the same seed was used while in (**c**) a different seed was used for the random initial conditions. The same amplitude and size of stripe is obtained, but this time it is horizontal instead of vertical. (From Tyson 1996)

The remaining parameters are μ, β and w. So, we need to explore the (β, μ), (μ, w) and (β, w) parameter spaces. We are dealing with a four-dimensional parameter space but it is three-dimensional for given ρ. At this point we can marginally simplify the system by setting

$$\bar{\delta} = \frac{\delta w^2}{1 + w^2}, \quad \bar{\beta} = \beta w \tag{5.83}$$

and rewriting the model as

$$\frac{\partial u}{\partial t} = d_u \nabla^2 u - \alpha \nabla \left[\frac{u}{(1+v)^2} \nabla v \right] + \rho u(\bar{\delta} - u)$$
$$\frac{\partial v}{\partial t} = \nabla^2 v + \bar{\beta} \frac{u^2}{\mu + u^2} - uv. \tag{5.84}$$

This simplifies the algebra considerably, but still lets us determine the effect of increasing or decreasing w by mapping points (β, δ) to $(\bar{\beta}, \bar{\delta})$ as w increases using (5.81). This mapping is a sigmoidal curve for each (β, δ) pair in the $(\bar{\beta}, \bar{\delta})$ plane.

With this formulation the unknown parameters are β, δ and μ. If we fix μ to be large compared with u^2, we recover the simplified model (5.80) that we just considered. Surprisingly, $\bar{\beta}$ does not need to be very much larger than β for this pattern domain to be recovered. For smaller values of μ, the pattern domain is different. An example is shown in Figure 5.15.

Tyson (1996) carried out simulations for parameters from the stripes, spots and indeterminate regions and these confirmed the analytical predictions as to which pattern type will be found in small periodic domains subject to small random perturbations of the steady state. Interestingly she also found that steady state patterns exist in at least part of the indeterminate region, where the analysis can not, as yet, predict what patterns will occur. An explanation for the latter is an interesting analytical problem. Examples of these patterns are shown in Figure 5.16.

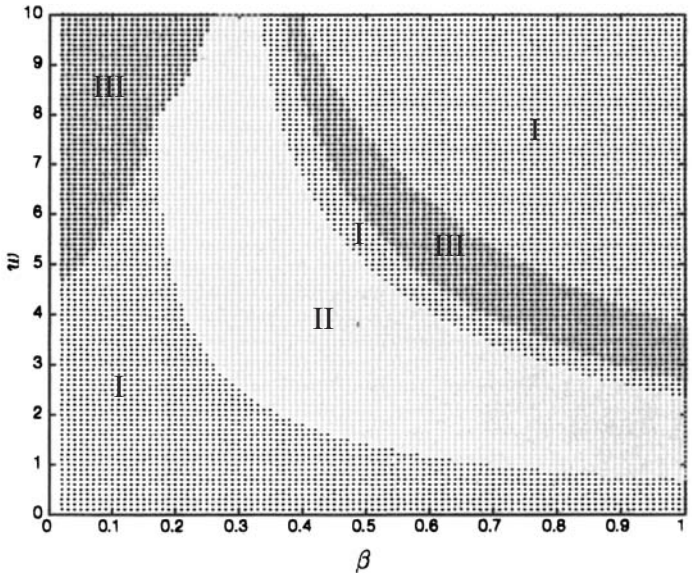

Figure 5.15. The pattern domain for the full model without w. The parameter values are $d_u = 0.25, \alpha = 90.0$ and $\mu = 1000.0$. As $\bar{\beta}$ and $\bar{\delta}$ (defined by (5.83))are varied, the corresponding value of ρ is determined from equation (5.82). The perturbation parameter is β. The pattern regions give stripes (I), spots (II) and indeterminate patterns (III). (From Tyson 1996)

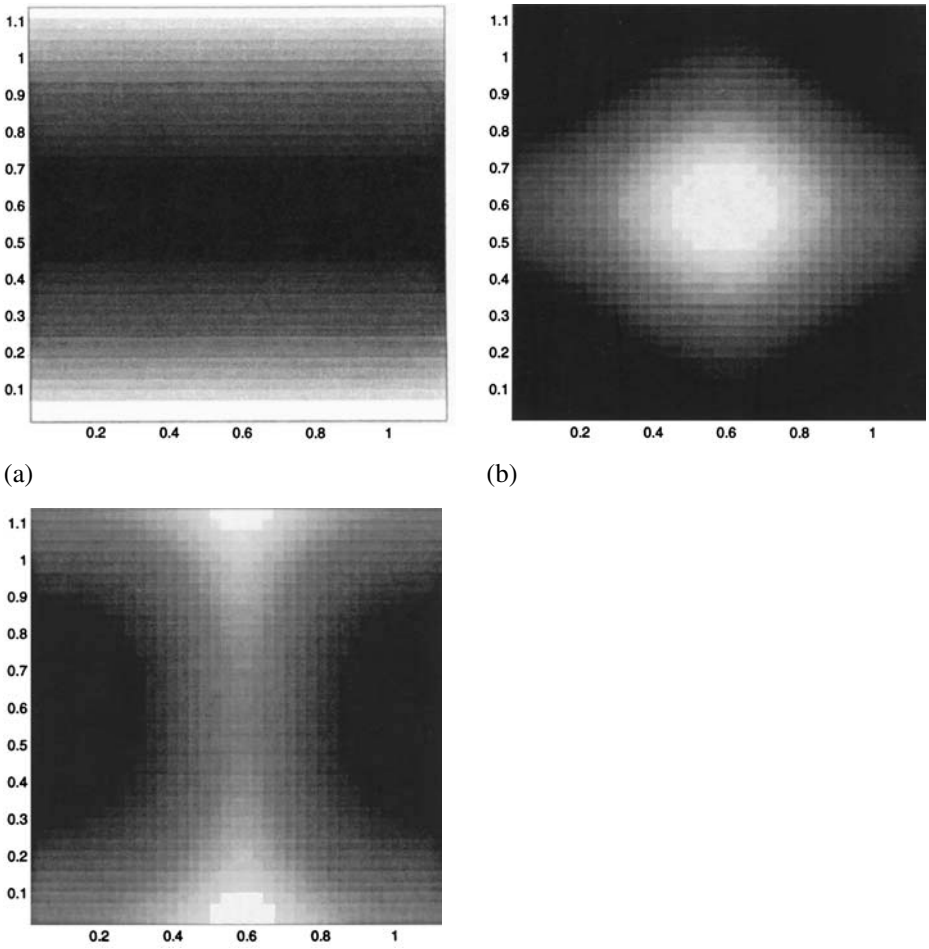

Figure 5.16. Simulations of the full equations for parameters in the domains which predict the various patterns. Light regions denote high cell density. In each case the domain chosen can sustain one 2π oscillation. The perturbation was $\varepsilon = 0.1$. The parameter values are $d_u = 0.25$, $\alpha = 90.0$, $\bar{\beta} = 10.0$, $\mu = 100.0$; then (**a**) Stripe: $\bar{\delta} = 4.6$, $\rho = 8.5133$, $u_0 = u^* = 4.6$, $v_0 = v^* = 0.3797$ and $l_x = l_y = l = 1.213$; (**b**) Spot: $\bar{\delta} = 5.1$, $\rho = 7.797$, $u_0 = u^* = 5.1$, $v_0 = v^* = 0.4747$ and $l_x = l_y = l = 1.177$; (**c**) Indeterminate pattern: $\bar{\delta} = 5.5$, $\rho = 7.139$, $u_0 = u^* = 5.5$, $v_0 = v^* = 0.4233$ and $l_x = l_y = l = 1.159$. (From Tyson 1996)

5.9 Numerical Results with Initial Conditions from the Experiments

The nonlinear analysis of the semi-solid models we discussed above only applies to small random perturbations of the uniform positive steady state. The initial conditions in the experiments are, as described in Section 5.1, completely different. Initially there is no chemoattractant present, and only a small localised inoculum of cells which is a relatively large perturbation of the uniform zero steady state. We also have zero flux boundary conditions on a large domain, rather than periodic boundary conditions on a

small domain. The bacterial lawn preceding the pattern establishes conditions relevant to the nonlinear behaviour. So, with the experimental initial conditions we expect to find rings in the stripes region of the pattern domain, and broken (spotted) rings in the spots region. Tyson (1996) carried out extensive simulations in both one and two dimensions with parameters in the various regions which give spots and stripes. Here we give some of her results and some of those presented by Tyson et al. (1999).

We start with the simplified semi-solid model (5.80) in one dimension. With the same parameter values as in Figure 5.14 which gave a stripe pattern we again get a series of concentric rings. In the case of the parameter values which gave a spot pattern only a few small pulses appeared near the the initial disturbance which slowly decayed. It seems that the spotted ring patterns obtained experimentally arise either from the stripes region of the nonlinear analysis pattern domain, or from some pattern region completely outside the predictions of the nonlinear analysis. In no way did we obtain the complete patterning scenario from the nonlinear analysis.

Even a cursory investigation of parameter space showed that we need not restrict ourselves to parameters from the nonlinear analysis to find interesting patterns and how patterns vary with parameter variation. For example, if we increase the chemotaxis coefficient α, the amplitude increases as well as the wavelength of the stripes. A small increase in nutrient concentration w, increases the propagation speed and causes the pulses behind the wavefront to decay. Only a slightly larger increase in w makes the pulses disappear altogether, as the cell density rapidly approaches the uniform positive steady state. Pulses still form for decreased levels of w, but the pattern propagates more slowly. The rate of growth, ρ, affects the pattern in exactly the same way as nutrient concentration. A factor of two decrease in chemoattractant production β increases both the amplitude and the frequency of pulses. The carrying capacity δ is directly related to the amplitude of the pattern and also the length of time it takes to form. The permutations are endless.

In two dimensions, simulations were run with the parameters which gave stripes from the nonlinear analysis and the simulation gave concentric rings. The wavelength of the radial pattern is smaller in two dimensions than that in one dimension, and the amplitude is about the same. The spacing between rings does not change as the radius increases as shown in Figure 5.17.

Increasing the chemotaxis parameter from $\alpha = 2.25$ to $\alpha = 5$ in two dimensions we get a series of concentric rings made up of spots. A time sequence of the pattern is shown in Figure 5.18 together with a surface plot of the solution at $t = 70$. As in one dimension, increasing the chemotaxis coefficient increases both the wavelength and amplitude of the pattern. Importantly we found that nutrient consumption does not change a spot pattern to a stripe pattern, nor does it change the wavelength.

We now consider the full model system (5.84) which introduces one more parameter, namely, μ which measures saturation level of chemoattractant production. From the simple model we found that varying the parameters α, β, ρ, δ and κ can change a pattern of concentric rings. Basically the full model gives the same patterns found in the simple model but with certain quantitative differences as we would expect. Trivially, for the saturation level of chemoattractant production, μ, sufficiently large and little consumption of nutrient, the full model essentially reduces to the simple one and behaves in exactly the same way. More importantly, for parameters which allow more of the

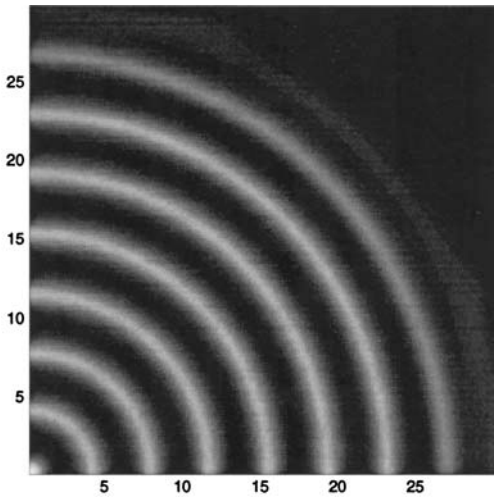

Figure 5.17. Simulation results for the model system (5.80) with the same parameters as in Figure 5.14(b) but with initial conditions like those of the semi-solid experiments. The parameter values are: $d_u = 0.25$, $\alpha = 2.25$, $\beta = 0.2$, $\mu = 1.0$, $\delta = 20.0$, $\rho = 0.01$, $w = 1.0$, $u_0 = u^* = 5.0$ at the bottom left corner and $v_0 = 0.0$. (From Tyson 1996)

middle and saturating portions of the aspartate production curve to play a part in the simulations, we also find continuous and spotted rings as shown in Figures 5.19(a) and (b). Adding consumption of food does not change the nature of the ring pattern, except to make it gradually disappear from the centre outwards.

Relation of the Simulations to the Experiments

The simulation results compare remarkably well with the experimental results obtained for *S. typhimurium* and described in Section 5.1. The pattern is preceded by a bacterial lawn of low cell density. Each ring forms at a discrete radial distance from the previous one, and then remains stationary. The spotted rings form first as continuous rings which subsequently break up into spots. All of these traits obtained from the model mechanism are characteristic of the *S. typhimurium* patterns.

If we take the parameter values from Figure 5.19(b) we get

$$k_7 = \frac{k_3}{\rho} = 1.6 \times 10^{-9} \text{ ml (cell hr)}^{-1}$$

$$x = x^* \sqrt{\frac{D_c}{k_7 n_0}}.$$

Four rings form in a distance $x^* = 10$ which corresponds to $x = 1.4$ cm, which is close to the experimentally observed value of $x \approx 1$ cm (Woodward et al. 1995).

5.10 Swarm Ring Patterns with the Semi-Solid Phase Model Mechanism

The most dramatic patterns observed by Budrene and Berg (1991) arise from an expanding high-density ring of bacteria called a swarm ring. These patterns were described and

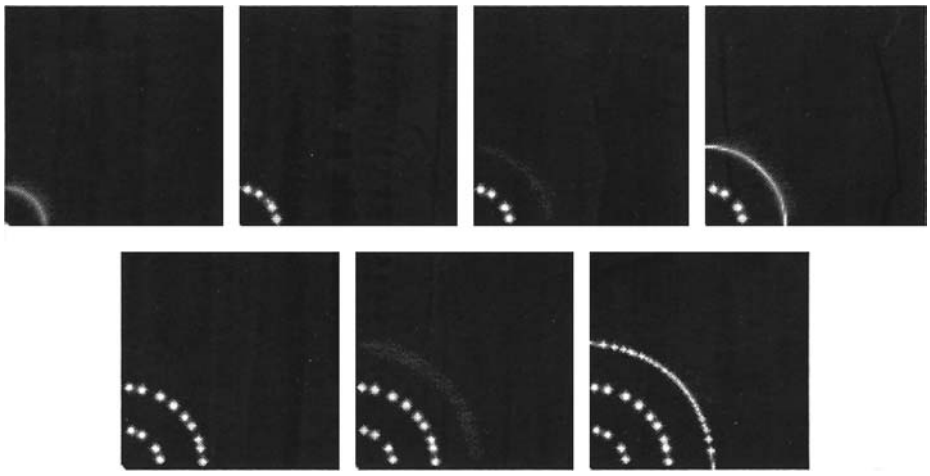

(a)

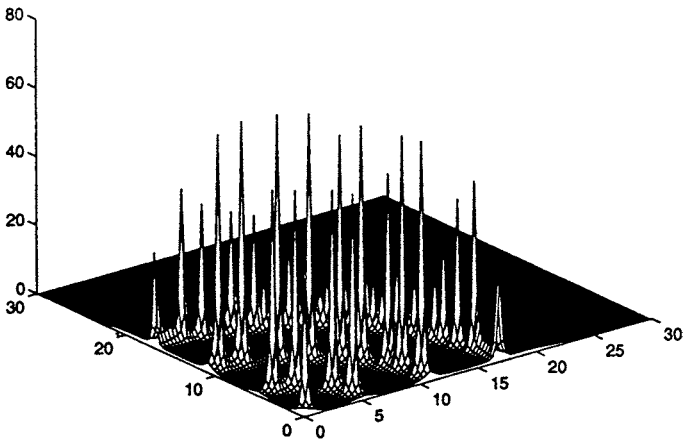

(b)

Figure 5.18. Simulation results for the model system (5.80) with the same parameters as in Figure 5.16(b) (and in Figure 5.14) but with initial conditions like those of the semi-solid experiments except that here $\alpha = 5$. Again the initial cell density was zero everywhere except for a small inoculum of maximum density 5 at the origin; the initial chemoattractant concentration was zero everywhere and the initial nutrient concentration was 1 everywhere. Solutions are shown in time increments of $t = 5$ from $t = 40$ to 70. The last figure is a surface plot of the data presented in the final image when $t = 70$. (From Tyson 1996)

illustrated in Section 5.1. The initial conditions are a localised inoculum of cells on a dish containing a uniform distribution of food and no chemoattractant, and the boundary conditions are zero flux.

Since the patterns begin with a continuous swarm ring, which only later leaves behind a pattern with angular variation, it is natural to study first a travelling wave or pulse in the one-dimensional version. The initial configuration is a uniform concentration of food and a dense inoculum of bacteria at one place. There is no chemoattractant present.

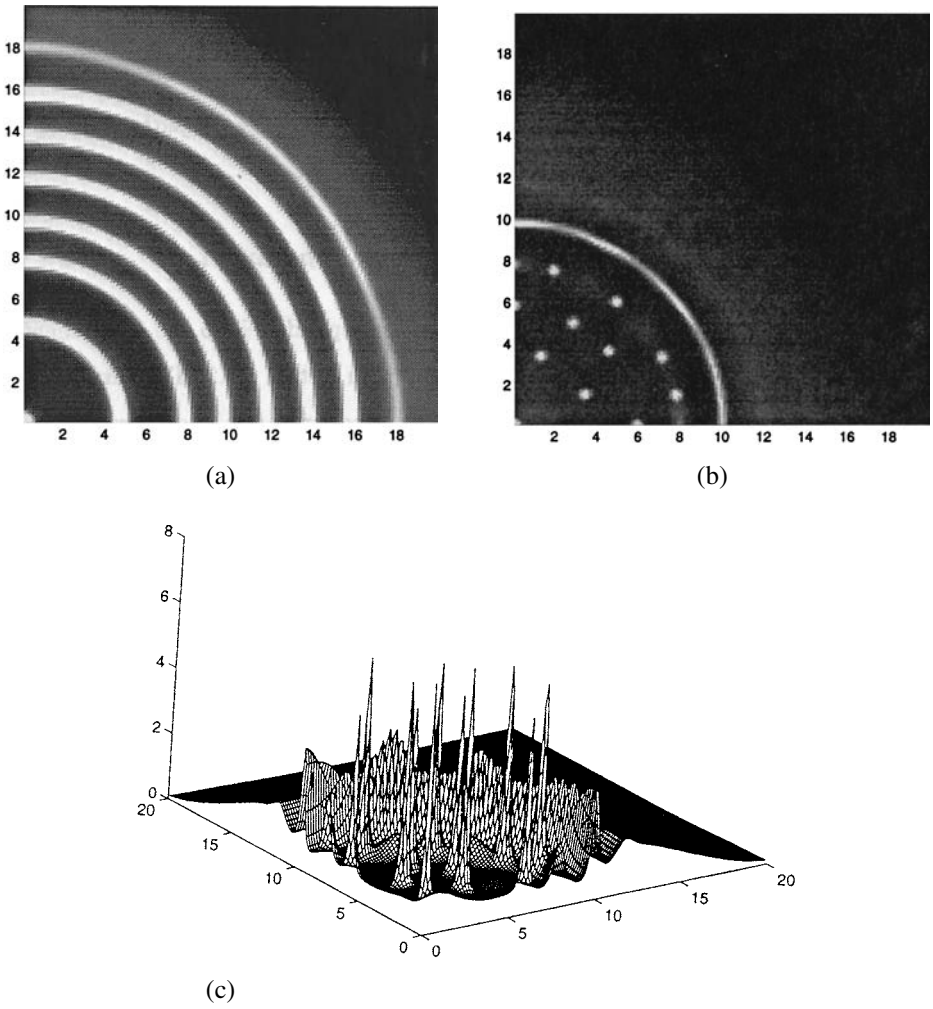

Figure 5.19. (**a**) Continuous rings obtained from numerical simulation of the full model. Parameter values: $d_u = 0.25$, $\alpha = 7.0$, $\beta = 10.0$, $\mu = 250$, $\delta = 10.0$, $\rho = 0.1$, $w = 5.0$. (**b**) Spotted rings obtained with parameter values: $d_u = 0.25$, $\alpha = 30.0$, $\beta = 10.0$, $\mu = 50$, $\delta = 10.0$, $\rho = 1.0$, $w = 0.8$, $\kappa = 0.1$. Note the interdigitation of the spots in successive rings. (**c**) Surface plot of the spotted ring pattern in (**b**). (From Tyson 1996)

The simplest swarm ring can form in the absence of chemoattractant production. As time increases, the bacteria consume the food and diffuse outwards. Those left in the middle become non-motile. At the outer edge of the diffusing mass of cells, the cell density is low and the food concentration is high and as a result the cells proliferate, increasing the local cell density. Meanwhile, at the centre of the spot where the cells were initially placed, the food has been consumed and its concentration reduced to the point where cell death dominates. The result is that cell numbers decrease at the location of the initial inoculum, and increase at the diffusing front. This situation evolves to produce a travelling pulse.

The addition of chemoattractant can make the smooth swarm ring unstable. It is reasonable to suppose that the instability can nucleate more complicated geometries in one, and even more, so in two dimensions, and in particular can give rise to the spots observed trailing the swarm ring in experiments.

We studied this phenomenon analytically in detail. We began by looking for one-dimensional travelling pulse solutions in the simplified version of the model and looked for solutions in terms of the travelling wave coordinate $z = x - ct$, where c is pulse propagation speed which has to be determined. We start with the semi-solid model equations (5.38)–(5.40) and, writing $u(x,t) = U(z)$, $v(x,t) = V(z)$ and $w(x,t) = W(z)$, the travelling waveforms of the equations become

$$\begin{aligned} &d_u U'' + cU' - \alpha\left[\frac{U}{(1+V)^2}V'\right]' + \rho U\left(\delta\frac{W^2}{1+W^2} - U\right) = 0 \\ &V'' + cV' + \beta W\frac{U^2}{\mu+U^2} - UV = 0 \\ &d_w W'' + cW' - \kappa U\frac{W^2}{1+W^2} = 0, \end{aligned} \tag{5.85}$$

where prime denotes differentiation with respect to z. Equations (5.85) can be written as a first-order system of 6 equations for U, U', V, V', W, W' with steady states

$$(U, U', V, V', W, W') = (0, 0, 0, 0, 0, 0) \tag{5.86}$$

and

$$(U, U', V, V', W, W') = (0, 0, 0, 0, W_0, 0). \tag{5.87}$$

The first is the steady state which exists behind the pulse, while the second is that which exists in front. Realistic solutions U, V and W must be non-negative and bounded, and so as we approach the two steady states the eigenvalues must be real so that there are no oscillations. Linearising equations (5.85) about (5.86) and (5.87) and solving for the eigenvalues, we find that the first steady state is always a focus. For the second to be a focus as well, we must have

$$c \geq c_{\min} = 2\sqrt{d_u \rho \delta W_0} \tag{5.88}$$

For the Fisher–Kolmogoroff equation, with appropriate initial conditions (namely, compact support) that we studied in detail in Chapter 13, Volume I we showed that a stable travelling wave solution evolves with speed $c_{\min}$. The experiments effectively imply such initial conditions so we suppose that the travelling pulse solution to equations (5.85) will also travel at or near $c_{\min}$. Interestingly neither the rate of food consumption, κ, nor the chemotaxis coefficient, α, have any effect on $c_{\min}$; according to the linear analysis it is purely the kinetics of the diffusing and proliferating bacteria which determine the pulse speed.

Stability of the Swarm Ring

Once the swarm ring has formed and starts to expand across the petri dish, it has been observed experimentally that the ring periodically breaks up, leaving behind a pattern of spots. This suggests that mathematically we should look for a swarm ring solution which is locally stable to perturbations in the radial direction and locally unstable to perturbations in the angular direction.

In the following we sketch how it might be possible to get some stability information on these swarm rings. So that the analytical suggestions mimic the experimental arrangement, we consider a rectangular domain (for analytical convenience), with the initial inoculum of cells placed along one edge of length l. Perpendicular to that edge we expect the solution to be a travelling pulse. We rewrite the two-dimensional model in (x, y, t) coordinates in terms of one travelling pulse coordinate, z, the coordinate parallel to the front, y, and so the equations (5.38)–(5.40) become

$$\begin{aligned}
\frac{\partial u}{\partial t} - c\frac{\partial u}{\partial z} &= d_u\left(\frac{\partial^2 u}{\partial z^2} + \frac{\partial^2 u}{\partial y^2}\right) - \alpha\left(\frac{\partial}{\partial z}, \frac{\partial}{\partial y}\right)\cdot\left[\frac{u}{(1+v)^2}\left(\frac{\partial v}{\partial z}, \frac{\partial v}{\partial y}\right)\right] \\
&\quad + \rho u\left(\delta\frac{w^2}{1+w^2} - u\right) \\
\frac{\partial v}{\partial t} - c\frac{\partial v}{\partial z} &= \left(\frac{\partial^2 v}{\partial z^2} + \frac{\partial^2 v}{\partial y^2}\right) + \beta\frac{wu^2}{\mu+u^2} - uv \\
\frac{\partial w}{\partial t} - c\frac{\partial w}{\partial z} &= d_w\left(\frac{\partial^2 w}{\partial z^2} + \frac{\partial^2 w}{\partial y^2}\right) - \kappa\frac{uw^2}{1+w^2}.
\end{aligned} \tag{5.89}$$

Now suppose that in the z-direction we have a travelling wave solution $U(z, y) = U(z)$, $V(z, y) = V(z)$, $W(z, y) = W(z)$ $\forall\ y \in [0, l]$. Then by definition,

$$\begin{aligned}
-c\frac{\partial U}{\partial z} &= d_u\left(\frac{\partial^2 U}{\partial z^2}\right) - \alpha\left(\frac{\partial}{\partial z}\right)\cdot\left[\frac{U}{(1+V)^2}\left(\frac{\partial V}{\partial z}\right)\right] \\
&\quad + \rho U\left(\delta\frac{W^2}{1+W^2} - U\right) \\
-c\frac{\partial V}{\partial z} &= \left(\frac{\partial^2 V}{\partial z^2}\right) + \beta\frac{WU^2}{\mu+U^2} - UV \\
-c\frac{\partial W}{\partial z} &= d_w\left(\frac{\partial^2 W}{\partial z^2}\right) - \kappa\frac{UW^2}{1+W^2}.
\end{aligned} \tag{5.90}$$

If this solution is stable to perturbations in z, as it is likely to be for some range of parameters, then we could get some idea of the effect of perturbations perpendicular to the direction of the wave by looking at spatiotemporal perturbations involving only the

spatial coordinate y. So as a first attempt at such a stability analysis we could consider the solutions u, v and w of the form

$$\begin{aligned} u(z, y, t) &= U(z) + \bar{u}e^{\lambda t + iky} \\ v(z, y, t) &= V(z) + \bar{v}e^{\lambda t + iky} \\ w(z, y, t) &= W(z) + \bar{w}e^{\lambda t + iky}, \end{aligned} \tag{5.91}$$

where $\bar{u}$, $\bar{v}$ and $\bar{w}$ are small constants. Substituting these forms into equations (5.89) and collecting terms of $O(\bar{u})$, $O(\bar{v})$ and $O(\bar{w})$ we would obtain a linear system of equations of the form

$$A \begin{bmatrix} \bar{u} \\ \bar{v} \\ \bar{w} \end{bmatrix} e^{\lambda t + iky} = 0, \tag{5.92}$$

where the matrix A is given by

$$A = \begin{bmatrix} \lambda + d_u k^2 - H_1 & H_2 & -\rho\delta \frac{2UW}{(1+W^2)^2} \\ -\beta\mu \frac{2WU}{(\mu+U^2)^2} + V & \lambda + k^2 + U & -\beta \frac{U^2}{\mu+U^2} \\ \kappa \frac{W^2}{1+W^2} & 0 & \lambda + d_w k^2 + \frac{2\kappa UW}{(1+W^2)^2} \end{bmatrix}, \tag{5.93}$$

where

$$\begin{aligned} H_1 &= \rho \left(\frac{\delta W^2}{1+W^2} - 2U \right) + \alpha \left[\frac{V'}{(1+V)^2} \right]', \\ H_2 &= -\frac{\alpha U k^2}{(1+V)^2} - 2\alpha \left[\frac{UV'}{(1+V)^3} \right]'. \end{aligned} \tag{5.94}$$

In the now usual way, nonzero solutions exist for the perturbations $\bar{u}$, $\bar{v}$ and $\bar{w}$ if and only if $|A| = 0$ which gives the characteristic equation for the dispersion relation λ. Setting $|A| = 0$ we get a cubic equation for λ of the form

$$\lambda^3 + A\lambda^2 + B\lambda + C = 0, \tag{5.95}$$

where the A, B and C are functions of the parameters, the wavenumber k and functions of z via the travelling wave solutions U, V, W and their derivatives. If we suppose, for the moment that A, B and C are constants, the Routh-Hurwitz conditions (see Appendix A, Volume 1) which guarantee $Rl(\lambda) < 0$ are

$$A > 0, \quad C > 0, \quad AB - C > 0. \tag{5.96}$$

So, to ensure instability, namely $Rl(\lambda) > 0$ for some $k^2 \neq 0$ at least one of these conditions must be violated. We rewrite the coefficient matrix A of (5.93) as

$$\begin{bmatrix} \lambda + c_1 & c_4 & -c_5 \\ c_6 & \lambda + c_2 & -c_7 \\ +c_8 & 0 & \lambda + c_3 \end{bmatrix}, \tag{5.97}$$

where the terms which are always negative have a minus sign in front and those which are clearly positive have a plus sign. With this notation (5.95) then has

$$\begin{aligned} A &= c_1 + c_2 + c_3, \\ B &= c_1c_2 + c_1c_3 + c_2c_3 - c_4c_6 + c_5c_8, \\ C &= c_1c_2c_3 - c_4(c_6c_3 + c_7c_8) + c_5c_2c_8. \end{aligned} \tag{5.98}$$

Now consider the three necessary conditions for stability. With A, the only term which can be negative is c_1, and this can occur only if H_1 in (5.94) is sufficiently large. But this depends on z and hence where we are on the travelling wavefront. Similar arguments apply to the other conditions of stability. It is clear then that whether or not the travelling wavefront, the swarm ring, is unstable to transverse perturbations depends on the travelling wave variable z. It would be astonishing if, for at least some z, it was not possible to violate the conditions (5.96) and hence have $Rl\lambda > 0$ for nonzero wavenumbers and transverse spatial instabilities which imply the breaking up of the swarm ring into spots. Since the chemotaxis parameter α appears in H_1 and H_2 it is clear that once again chemotaxis plays a critical role. A full analysis of the stability of these swarm rings is a challenging unsolved problem.

Tyson (1996) solved the one-dimensional equations and obtained a single travelling pulse or a train of two to four travelling pulses from the full model for a variety of parameter values, and nonnegligible consumption of nutrient. The effect of the model parameters α, β, μ, δ, ρ and w on the travelling pattern is analogous to their effect on the stationary patterns that we discussed above. The wavelength of the pulses in the pulse train is affected chiefly by the chemotaxis coefficient α.

The predicted and numerically computed wavespeeds compare very well. The computed wavespeed was always larger (around 5–10%) than the predicted value, $c_{\min}$, as it should be. Since necessarily boundary conditions had to be imposed on a finite domain, we do not expect the wavespeed to be as small as $c_{\min}$ in our simulations.

Numerical Results for Two-Dimensional Swarm Rings

In two dimensions, we found that the travelling pulse trains become a swarm ring followed by one or two rings of spots. The spots arise from inner rings which develop angular instabilities and subsequently break up into spots. Image plots of a well-developed swarm ring pattern are shown in Figure 5.20 at various times in their development.

This model development and analysis was the first mathematical model of *E. coli* and *S. typhimurium* which yielded a swarm ring spawning spots without assuming any extraneous biological activity. Woodward et al. (1995) obtained interesting patterns by assuming the presence of a chemoattracting nutrient. Experiments with *S. typhimurium* have been performed under such circumstances, but in the *E. coli* experiments no such nutrient is present. With this model, we have shown that chemotaxis toward the aspar-

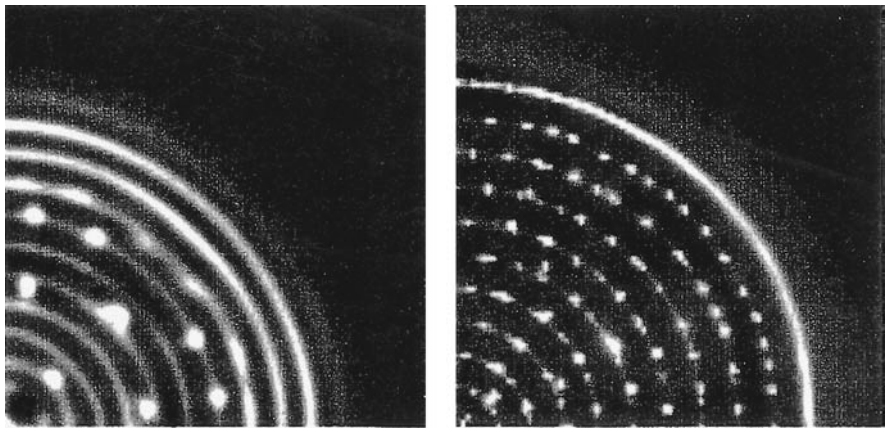

Figure 5.20. Swarm ring patterns in *S. typhimurium* obtained from a numerical simulation of the full system (5.38)–(5.40): (**a**) Concentric rings showing transition to a spotted ring pattern. Parameter values: $d_u = 0.25$, $d_w = 0.8$, $\alpha = 40$, $\beta = 10$, $\delta = 70$, $\rho = 1$, $\kappa = 4.5 \times 10^{-3}$, $\mu = 10^2$. (**b**) Concentric spotted rings. Parameter values: $d_u = 0.26$, $d_w = 0.89$, $\alpha = 88.9$, $\beta = 8$, $\delta = 7$, $\rho = 1$, $\kappa = 10^{-3}$, $\mu = 10^2$. (From Tyson 1996)

tate produced by the cells coupled with consumption of food are sufficient to generate the experimentally observed behaviour. This is in keeping with the experimentalists' intuition.

5.11 Branching Patterns in *Bacillus subtilis*

The patterns we have discussed above are complex, but fairly regular patterns formed by spots and rings. The bacterium *Bacillus subtilis*, when inoculated onto a agar medium which has little nutrient, can exhibit quite different fractal-like patterns not unlike those found in diffusion-limited aggregation (see, for example, Matsuyama and Matsushita 1993). When the agar is semi-solid, however, the bacterial colonies formed by *Bacillus subtilis* are dense-branching patterns enclosed by a smooth envelope. The stiffness of the medium affects the patterns formed. Shigesada and her colleagues (Kawasaki et al. 1997) have studied this particular bacterium and constructed a relatively simple reaction diffusion model which captures many of the pattern characteristics found experimentally: they compare the results with experiments. Here we briefly describe their model and show some of their results. Although their model is a reaction diffusion one it is original and fundamentally different to those reaction diffusion systems we have studied up to now. It highlights, once again, the richness of pattern formation by such relatively simple systems.

They propose a model consisting of a conservation equation for the bacterial cells and the nutrient given by

$$\frac{\partial n}{\partial t} = D_n \nabla^2 n - \frac{knb}{1 + \gamma n} \tag{5.99}$$

$$\frac{\partial b}{\partial t} = \nabla \cdot (D_b \nabla b) + \theta \frac{knb}{1+\gamma n}, \quad D_b = \sigma nb, \tag{5.100}$$

where n and b are the concentration of the nutrient and bacterial cell densities respectively. Here the function $knb/(1+\gamma n)$, where k and γ are constants, is the consumption rate of the nutrient by the bacteria and $\theta(knb/(1+\gamma n))$ is the growth rate of the cells with θ the conversion rate factor. D_n and D_b are the diffusion coefficients of the nutrient and cells respectively. We now motivate the form given for D_b.

The reasoning behind the form $D_b = \sigma nb$ is based on the work of Ohgiwara et al. (1992) who observed the detailed movement of the bacteria and found that the cells did not move much in the inner region of the expanding colony where the level of nutrient was low but that they moved vigorously at the periphery of the colony where the nutrient level is much higher. They also noted that at the outermost front of the colony, where the cell density is quite low, the cells were again fairly inactive. Kawasaki et al. (1997) then argued that the bacteria are immobile where either the nutrient n or the bacteria density b are small. They modelled these effects by taking the bacterial diffusion as proportional to nb with the proportionality factor σ. It was also observed that although each cell moves in a typical random way some of them exhibit stochastic fluctuations. They quantified this by setting $\sigma = 1 + \Delta$ where the parameter Δ is a measure of the stochastic fluctuation from the usual random diffusion.

Kawasaki et al. (1997) studied the pattern formation potential of these model equations in two dimensions subject to initial conditions

$$n(\mathbf{x}, 0) = n_0, \quad b(\mathbf{x}, 0) = b_0(\mathbf{x}), \tag{5.101}$$

where n_0 is the concentration of the initial uniformly distributed nutrient and $b_0(\mathbf{x})$ is the initial inoculum of bacteria. Since the nutrient concentration in the experiments is relatively low the saturation effect, accounted for by the γn term, is negligible so the consumption of nutrient can be taken as approximately knb, the functional form we use below.

We nondimensionalise the equations by setting

$$n^* = \left(\frac{\theta}{D_n}\right)^{1/2} n, \quad b^* = \left(\frac{1}{\theta D_n}\right)^{1/2} b, \quad \gamma^* = \left(\frac{D_n}{\theta}\right)^{1/2} \gamma \tag{5.102}$$

$$t^* = k(\theta D_n)^{1/2} t, \quad \mathbf{x}^* = \left(\frac{\theta k^2}{D_n}\right)^{1/4} \mathbf{x}, \tag{5.103}$$

with which the model mechanism becomes, using the above consumption approximation with $\gamma = 0$, and omitting the asterisks for algebraic simplicity,

$$\frac{\partial n}{\partial t} = \nabla^2 n - nb \tag{5.104}$$

$$\frac{\partial b}{\partial t} = \nabla \cdot (\sigma nb \nabla b) + nb, \tag{5.105}$$

which has only one parameter σ, with initial conditions

$$n(\mathbf{x}, 0) = \left(\frac{\theta}{D_n}\right)^{1/2} n_0 \equiv \nu_0, \quad b(\mathbf{x}, 0) = \left(\frac{1}{\theta D_n}\right)^{1/2} b_0(\mathbf{x}) \equiv \beta_0(\mathbf{x}). \tag{5.106}$$

Kawasaki et al. (1997) solved this system under a variety of different situations and found that the solutions exhibited a remarkable spectrum of complex patterns. Figure 5.21 shows some examples.

Kawasaki et al. (1997) also investigated the patterns formed when the stochastic parameter $\Delta = 0$. Patterns still form and still give rise to branching-like patterns but since there is no anisotropy they are much more regular and symmetric. In reality, of course, the small random perturbations in nutrient and bacterial densities would not result in such regular patterns as pointed out by Kawasaki et al. (1997).

Although the pattern evolves in two dimensions each tip essentially grows in one dimension except when they branch. This makes it possible to obtain some approximate analytical results for tip growth, and hence the colony growth, using the one-dimensional version of the model equations, namely,

$$\frac{\partial n}{\partial t} = \frac{\partial^2 n}{\partial x^2} - nb \tag{5.107}$$

$$\frac{\partial b}{\partial t} = \frac{\partial}{\partial x}\left(\sigma nb \frac{\partial b}{\partial x}\right) + nb. \tag{5.108}$$

The numerical simulation of these one-dimensional equations gave growth rates which compared well with those obtained from the two-dimensional equations. They made a further approximation to the model by substituting $\sigma_0 \nu_0 b$ and $\nu_0 b(1 - b/K)$ for σnb and nb in (5.108) to obtain the scalar equation in b, namely,

$$\frac{\partial b}{\partial t} = \frac{\partial}{\partial x}\left(\sigma_0 \nu_0 b \frac{\partial b}{\partial x}\right) + \nu_0 b(1 - b/K). \tag{5.109}$$

Here the growth of the bacteria is limited by the nutrient according to a typical logistic growth where K is the saturating level of the bacteria. If we consider (5.107) and (5.108) in the absence of diffusion we can add the equations, integrate and with $n + b = \nu_0$ we get the logistic form $db/dt = \nu_0 b(1 - b/\nu_0)$ for the bacteria and so we relate K to ν_0. The form of (5.109) is then the same as the equation we discussed in detail in Section 13.4 in Chapter 13, Volume I and which has an exact travelling wave solution with the wavespeed $v_{\text{colony growth}}$ given by

$$v_{\text{colony growth}} = \left(\frac{\sigma_0 \nu_0^3}{2}\right)^{1/2}. \tag{5.110}$$

This velocity is a very good approximation (a slight overestimate) for the velocity of colonial growth obtained from (5.107) and (5.108).

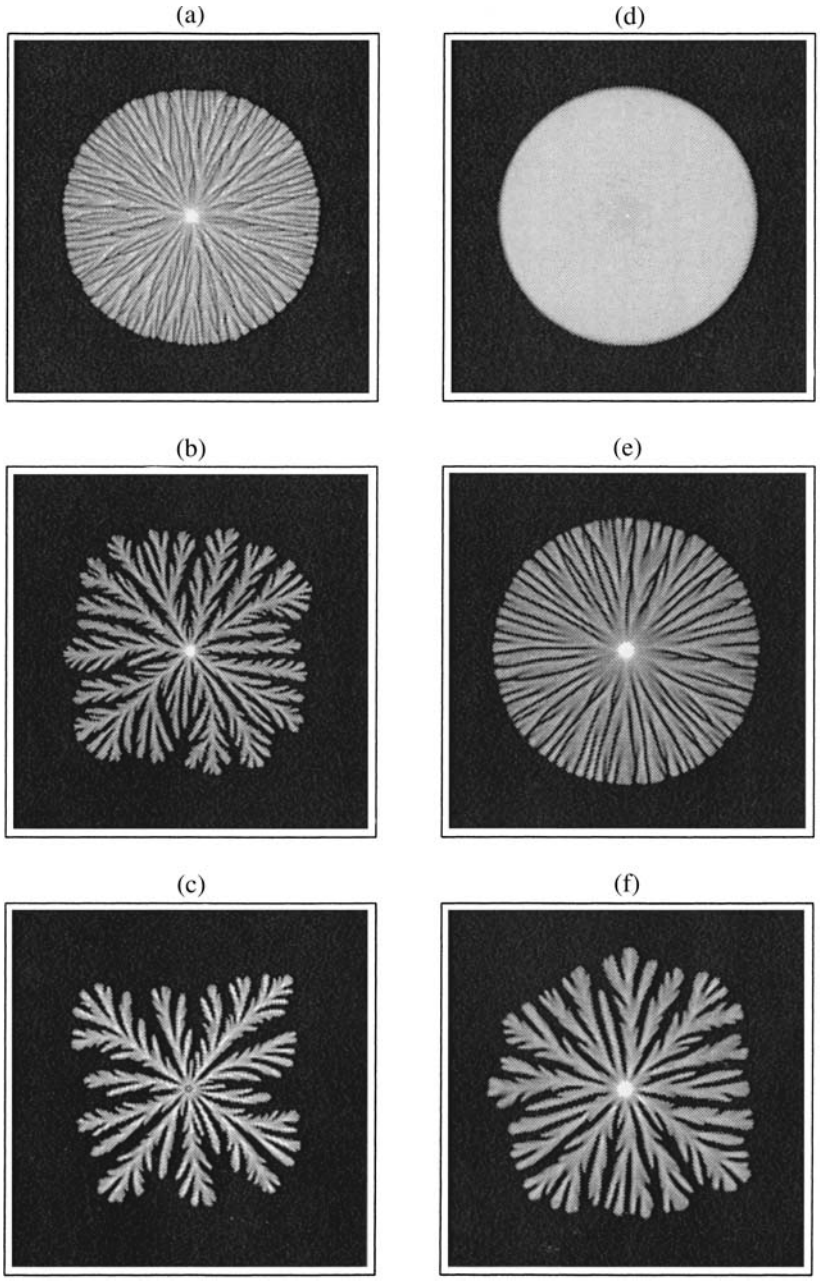

Figure 5.21. Typical dense-branching bacterial patterns for the *Bacillus subtilis* model obtained from a numerical simulation of (5.104)–(5.105). The parameter σ was perturbed about the mean σ_0 with the random variable Δ. Parameter values and times are: (**a**) $\sigma_0 = 1, \nu_0 = 1.07, t = 396$; (**b**) $\sigma_0 = 1, \nu_0 = 0.71, t = 2828$; (**c**) $\sigma_0 = 1, \nu_0 = 0.35, , t = 19233$; (**d**) $\sigma_0 = 4, \nu_0 = 1.07, t = 127$; (**e**) $\sigma_0 = 4, \nu_0 = 0.71, t = 566$, (**f**) $\sigma_0 = 4, \nu_0 = 0.35, t = 4525$. In real time the pattern is quite dense after about two days. (From Kawasaki et al. 1997 and reproduced with the permission of Dr. N. Shigesada)

When the nutrient level is not low the full model (5.99) and (5.100) has to be used with $\gamma \neq 0$. Kawasaki et al. (1997) considered such situations and found that as γ increases the branch width increases and the degree of complexity decreases. Their way of including a stochastic element is interesting and important since it allows for some stochasticity without the usual complexities involved in such studies. The concept clearly has a much wider application such as to many of the models studied in this book.